

The Effect of Prior Ferrite on Bainite Transformation Kinetics

Lennard Uittenbroek

A thesis presented for the degree of
Master of Science



3ME - Materials Science and Engineering

Delft University of Technology

The Netherlands

February 4, 2020

Acknowledgements

I want to thank the Technical University of Delft for teaching me and providing me with the knowledge and skills needed for this research and this thesis. Through the university I have learned much about materials science in the past few years.

Special thanks goes out to Dr. Ashwath M. Ravi and Prof.Dr. Maria J. Santofimia for guiding me through this project. Their time, patience, advice and remarks during our discussions were invaluable to the accomplishment of this work. They showed and taught me the practical side of approaching scientific problems. The great talks I had every other week with Ashwath kept me on the right track and helped me discover a great deal about scientific research. The guidance of both of them during the writing of this thesis is also highly valued.

In addition, I would like to thank Nico Geerlofs, Sander van Asperen (and assistants) and Richard Huizenga for their aid and advice during the experiments. I want to thank them for the time they took and the experience they shared to help me with this study.

Last but not least, I would like to thank my family, friends and loving girlfriend for their support since day one. It is unlikely that I would ever have come so far without them.

This page is intentionally left blank.

Abstract

In this work the effect of ferrite on the formation of bainite is studied. Different ferrite fractions of up to 25% were obtained through the application of three different intercritical annealing treatments to an Fe-0.2C-3Mn-2Si (wt%) steel. Two of the heat treatments consisted of an isothermal hold at temperatures between 835°C and 950°C, which was followed by slow cooling to a bainite formation temperature of 400°C. A third heat treatment included fast cooling from top temperatures between 810°C and 950°C to the same bainite formation temperature of 400°C. The heat treated material has been studied by means of dilatometry, optical microscopy, scanning electron microscopy and Vickers micro-hardness tests.

All of the involved ferrite fractions had an accelerating effect on bainite formation, when compared to samples where no prior ferrite was present. The accelerating effect was larger for smaller prior ferrite fractions. It is proposed that the amount of preferential nucleation sites for bainite is increased by the formation of prior ferrite and leads to an acceleration of bainite formation. The presence of a significant amount of silicon (2 wt%) prevented the formation of cementite and resulted in carbon enrichment of austenite during ferrite formation. For the evaluated ferrite fractions, the accelerating effect due to ferrite presence is greater than the decelerating effect caused by the carbon enrichment of austenite, the latter becoming stronger with increasing ferrite fraction. Additionally, it is proposed that, due to the increase in preferential nucleation sites, a large amount of bainite sheaves start to grow simultaneously. Together with the autocatalytic nucleation of new bainite sub-units, this could account for the high bainite formation rates that were observed in the presence of ferrite. A change in bainite morphology from degenerated upper bainite to granular bainite with increasing prior ferrite fractions was noticed. No significant difference in hardness was observed between the samples that contained prior ferrite, but the fully austenitised samples were slightly harder. It is expected that increasing ferrite fractions will result in a decrease in overall hardness, when macro-hardness tests would be applied.

Nomenclature

α	Ferrite, a bcc crystal structure
α_b	Bainitic ferrite, a bcc crystal structure present in acicular morphologies that form bainite
γ	Austenite, an fcc crystal structure
κ_p	Pre-exponential factor
df_{α_b}/dt	Bainite formation rate
A_1	Temperature where austenite starts to form during heating, assuming total equilibrium
A_3	Temperature where the sample has become fully austenitic during heating, assuming total equilibrium
A_{c1}	Temperature where austenite starts to form during heating
A_{c3}	Temperature where the sample has become fully austenitic during heating
A_{r3}	Start temperature of ferrite formation during cooling
B	Bainitic remains, a ferrite morphology resulting from intercritically annealed bainite
b	Blocky ferrite, a blocky ferrite morphology
B_s	Bainite start temperature
bcc	Body-centered cubic crystal structure
C	Continuous ferrite, a ferrite morphology consisting of multiple ferrite grains that have merged
C_γ	Carbon concentration in austenite
CCT	Continuous-cooling-transformation
CFB	Carbide free bainite
CR	Cooling rate
DLB	Degenerated lower bainite
DUB	Degenerated upper bainite
E	Elongated allotriomorph, an elongated ferrite morphology
EDM	Electrical discharge machining
f	Fraction of a certain phase
fcc	Face-centered cubic crystal structure
G	Gibbs free energy

<i>GB</i>	Granular bainite
<i>h</i>	Planck constant
<i>HR</i>	Heating rate
<i>HT</i>	Heat treatment
<i>HT – 1</i>	Heat treatment of type 1
<i>HT – 2</i>	Heat treatment of type 2
<i>HT – 3</i>	Heat treatment of type 3
<i>i1</i>	Irregular - type 1, an irregular ferrite morphology
<i>i2</i>	Irregular - type 2, an irregular ferrite morphology
<i>IRP</i>	Incomplete reaction phenomenon
<i>k</i>	Boltzmann constant
<i>LB</i>	Lower bainite
<i>LVDT</i>	Linear Variable Differential Transformer
<i>M_s</i>	Martensite start temperature
<i>MA</i>	Martensite-austenite, a mixture of martensite and austenite in the microstructures
<i>morph</i>	Morphology
<i>N</i>	Number of preferential nucleation sites for bainite
<i>Negl.</i>	Negligible
<i>P</i>	Parallel ferrite, a ferrite morphology consisting of parallel elongated ferrite grains
<i>PAGS</i>	Prior austenite grain size
<i>Q_A[*]</i>	Activation energy for autocatalytic bainite nucleation at the bainitic ferrite-austenite interface
<i>Q_G[*]</i>	Activation energy for grain boundary nucleation
<i>SEI</i>	Secondary electron imaging
<i>SEM</i>	Scanning electron microscopy
<i>T</i>	Temperature
<i>T</i>	Tree-like, a branched ferrite morphology
<i>T₀</i>	Temperature where the Gibbs free energies of austenite and ferrite are equal
<i>T'₀</i>	Modification of <i>T₀</i> which includes the strain energy
<i>TT</i>	Top temperature, the maximum temperature in a certain heat treatment
<i>TTT</i>	Time-temperature-transformation
<i>UB</i>	Upper bainite
<i>wt</i>	Weight

Contents

1	Introduction	1
1.1	Objective and Scope	1
1.2	Report Structure	3
2	Literature Review	4
2.1	Bainitic Steels	4
2.2	Phase Transformations in Steel	4
2.2.1	Ferrite	5
2.2.2	Austenite	7
2.2.3	Cementite	8
2.2.4	Bainite	8
2.3	Kinetics of Bainite Formation	11
2.3.1	Bainite Nucleation	11
2.3.2	Bainite Growth	12
2.3.3	Bainite Formation Rate	13
2.3.4	The Effect of Common Alloying Elements	14
2.4	The Effect of Ferrite on Bainite Formation	15
3	Experimental Methods	18
3.1	Material	18
3.2	Dilatometry	18
3.2.1	Critical Temperatures and the Lever Rule	20
3.2.2	Martensite Start Temperature	20
3.2.3	Equipment	21
3.3	Heat Treatments	22
3.4	Metallographic Preparation	25
3.5	Optical Microscopy	26
3.6	Scanning Electron Microscopy	26
3.7	Micro-Hardness Testing	28

4	Results and Discussion	29
4.1	Critical Temperatures	29
4.2	Prior Ferrite	30
4.2.1	Ferrite Fractions Before Cooling	30
4.2.2	Ferrite Fractions After Cooling to 400°C	33
4.2.3	Carbon Enrichment of Austenite	34
4.2.4	Ferrite Morphology	37
4.2.5	Segregation of Alloying Elements	41
4.2.6	Prior Ferrite Summary	43
4.3	Bainite Formation	44
4.3.1	Bainite Formation	44
4.3.2	Bainite Formation Kinetics	46
4.3.3	Bainite Morphology	51
4.4	Micro-hardness	55
5	Conclusions	57
6	Recommendations	59
A	Sample Cutting	69
B	Error in Dilatometry Data	71

Chapter 1: Introduction

1.1 Objective and Scope

Steel has been one of the most widely used structural materials for decades. It offers great flexibility in material properties, ranging from hard to soft, from low to high strength, from tough to brittle and from corrosive to stainless. The properties of steel can be fine-tuned until a desired combination is found. In addition, the main constituent, iron, is relatively abundant and the steel making process is relatively cheap. It is therefore not surprising that steel is the primary material choice for a variety of applications.

Being a popular material, much effort is put into researching new microstructures, alloy compositions and production routes. Currently, hundreds of different steel grades exist, each having its own characteristics. These steel grades are often roughly sorted into classes based on for example composition, strength or microstructure. One such class is bainitic steels. The bainite microstructure that characterises these steels offers a high strength without compromising on ductility (formability). This is a preferable combination for many structural applications and bainite has therefore been intensively studied in the past decades. However, its complicated microstructure does not readily reveal its secrets and the formation mechanism of bainite has been the topic of much debate for decades [1]. More research is needed in order to obtain a better understanding, which may lead to new alloys, enhanced material properties and improved processing conditions. The current work is designed to further increase this understanding by studying the effect of ferrite on the bainite transformation kinetics.

The efficiency of a heat treatment process can be improved by decreasing the time required to complete the process. This also applies to bainite formation and research is conducted in order to find a way to accelerate the formation of bainite. This would be particularly helpful in the case of continuous annealing lines, where a shorter heat treatment may result in a higher output. Accelerating the bainite formation is also useful with large components, where low temperature bainite heat treatments are applied which can last up to several days [2]. One way an increase of the bainite formation rate might be achieved is to form a certain fraction of ferrite prior to bainite formation [3, 4].

From the available literature it can be deduced that the effect of ferrite formation on the subsequent formation of bainite is not yet well understood. Both accelerating and retarding effects were observed by different authors [3–5] and more research is required to understand these contradictory effects of ferrite on subsequent bainite formation kinetics. It is very likely that different fractions of ferrite will have a different impact on the subsequent bainite transformation, as larger fractions have an increased impact on the remaining austenite, from where bainite forms. Large ferrite fractions will decrease the volume in which bainite can grow and, if cementite does not precipitate, will enrich the surrounding austenite in carbon. To understand the effect of ferrite on bainite formation, the ferrite fraction will be varied and the subsequent bainite formation rate will be compared with that of a bainite heat treatment without prior ferrite formation. Contrary to past studies [3–5], in this study intercritical annealing will be used as a means to obtain fractions of ferrite.

The key research question that will be addressed in this study can be stated as follows:

What is the influence of the ferrite fraction on bainite formation kinetics?

In order to provide an answer to this question, the following aspects will be dealt with:

- Obtaining different ferrite fractions through intercritical annealing and/or slow cooling
- Comparison of bainite formation rates between heat treatments with and without prior ferrite formation
- Determination of relation between ferrite fraction and bainite formation kinetics
- Determination of the influence of ferrite morphology on subsequent bainite formation kinetics
- Characterisation of bainite morphology considering the different heat treatments involved
- Estimation of the effect of prior ferrite on the mechanical properties of bainite

The study will be carried out on an Fe-0.2C-3Mn-2Si (wt%) steel and will involve the use of dilatometry, optical microscopy, scanning electron microscopy and micro-hardness testing.

1.2 Report Structure

This report is comprised of different sections. It starts with a *Literature Review*, which introduces bainite and the state-of-the-art on bainite related research. It also provides background information and motivation for the current research. It is followed by *Experimental Methods* where the used material, equipment and procedures are explained. The *Results and Discussion* section contains a visualisation of the experimental outcome and subsequent analysis. The observations are explained and statements are made. In *Conclusions*, the reader can find the answer to the research question and other notable outcomes of this study. The *Recommendations* section contains suggested topics and recommendations for future research. Any additional information can be found in the *Appendix*.

Chapter 2: Literature Review

In this chapter the available literature concerning the topic of this thesis will be reviewed. Basic concepts will be explained and a scientific basis will be created on which the rest of this work will be built.

2.1 Bainitic Steels

Bainitic steels offer a combination of high strength and ductility. Within this class, ultimate tensile strengths range from just below 700 MPa for steels with excellent weldability to 1600 MPa for high strength bainitic steels [6]. For the newly developed nanostructured bainitic steels tensile strengths exceeding the 2000 MPa have been reported, while maintaining ductilities between 5% and 30% elongation [6, 7].

Bainitic steels have found widespread applications in industry. For example, the automotive industry, where they can be found in the production of shafts, bolts and crash reinforcement bars [6, 8]. It is also a prime material in the production of rail for train tracks and for bearings [8]. In addition, bainite is used in the energy generation industry (turbines) due to its creep resistance [8]. Tests have shown that certain bainitic steel plates can resist the same impact as ‘conventional’ armour plates, while only needing half of the weight. This makes bainite also very suitable as a material for armour plating [7].

2.2 Phase Transformations in Steel

The ability of steel to adopt different microstructures as a result of thermal treatments makes it a very versatile material. Steel microstructures can consist of a single phase or a combination of phases. These phases differ in crystal structure, which is defined by the manner in which the atoms are arranged (examples are shown in Figure 2.1). Each microstructure has its own properties and can be combined with other microstructures to tune the overall properties of the steel in a desired direction. The microstructures and phases that can be formed also depend on the composition of the steel, with carbon content as a main determining factor. To get an idea about what phases can

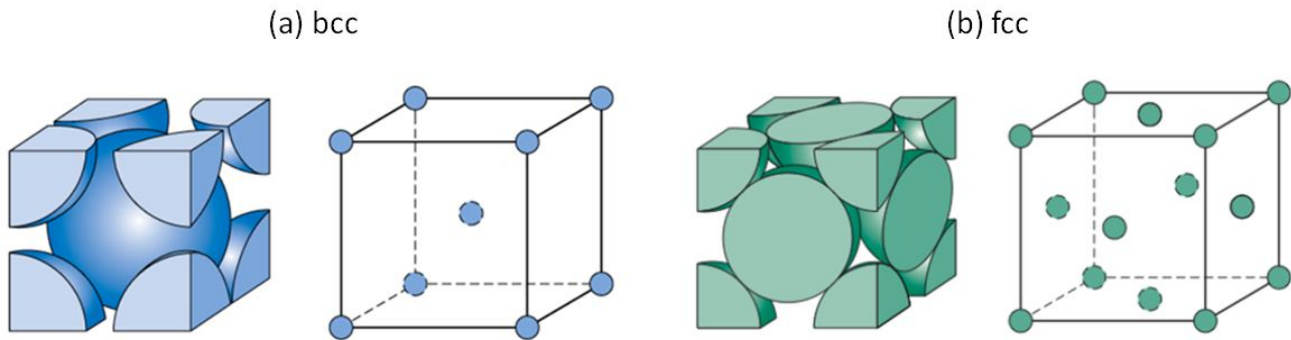


Figure 2.1: Schematic representations of the (a) bcc (ferrite) and (b) fcc (austenite) crystal structures [9].

be formed, the iron-carbon equilibrium phase diagram was developed. This diagram can be seen in Figure 2.2 and shows the most stable phase(s) for steel with a certain carbon content at a given temperature. For example, if a particular steel would have a carbon concentration of 0.2 wt% and it would be heated to 1000°C, it can be seen from Figure 2.2 that the austenite phase is expected to form. When this austenite is cooled down to temperatures below (approximately) 850°C, it can be seen that the austenite phase will (partly) transform into the ferrite phase. However, it is important to note that Figure 2.2 only shows the equilibrium structures, where the material is in full equilibrium and transformations and diffusive processes have come to a halt. In practice this condition is rarely met and the iron-carbon equilibrium phase diagram only serves to get an indication of the phase(s) that would form under equilibrium conditions. In addition, the presence of other alloying elements, such as manganese and silicon, will influence the shape of the curves in the iron-carbon equilibrium phase diagram.

Aside from the microstructures resulting from equilibrium phase transformations, a whole different range of microstructures can be created if the material is not allowed to achieve equilibrium. This can be done by increasing the cooling rate. To estimate the effect of cooling rate on the obtained microstructure Time-Temperature-Transformation (TTT) or Continuous Cooling Transformation (CCT) diagrams can be used. Figure 2.3 shows the additional microstructures that can be generated this way and it can be seen that a fast cooling rate will result in a different microstructure than would be formed with a slow cooling rate. So can martensite be formed by the application of a high cooling rate, while ferrite and pearlite can be formed with a slower cooling rate.

2.2.1 Ferrite

Ferrite is a phase that has the body-centered cubic (bcc) crystal structure shown in Figure 2.1a. It is stable at intermediate to low temperatures (see Figure 2.2) and is denoted as α . Ferrite is formed from austenite (γ) during cooling via nucleation and growth. Nucleation consists of small groups of atoms rearranging in the bcc structure [11]. The nucleation is heterogeneous and will take

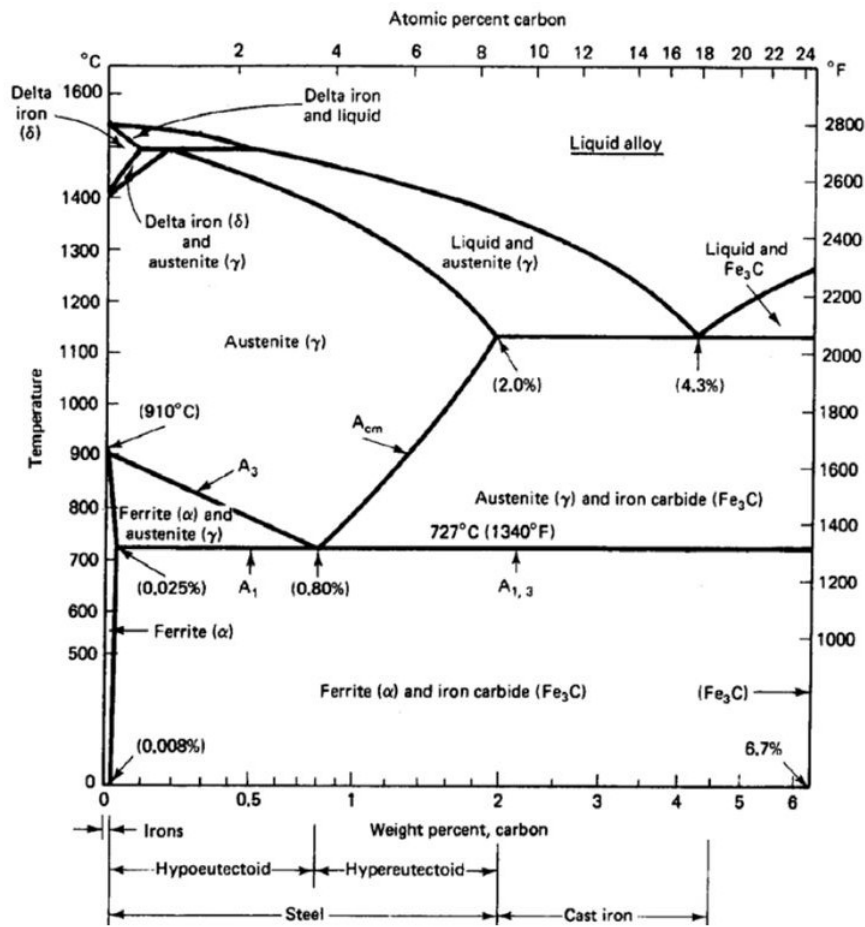


Figure 2.2: The iron-carbon equilibrium phase diagram [10].

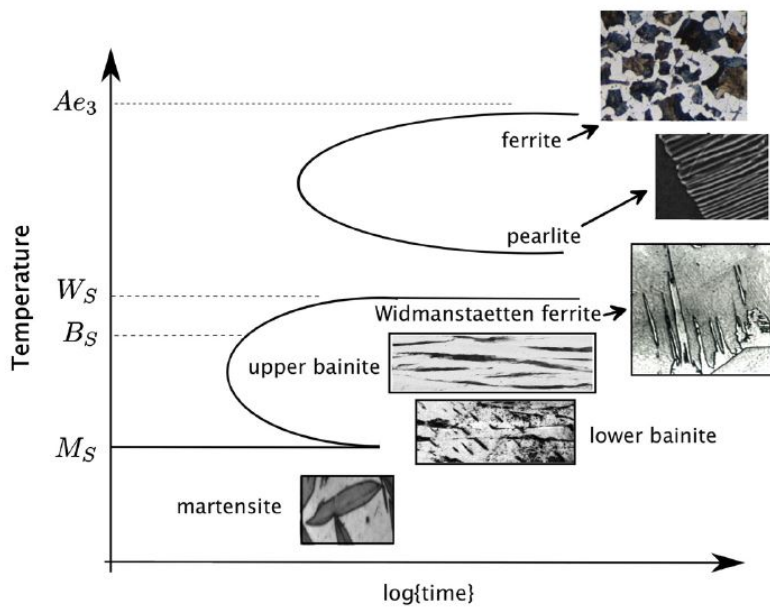


Figure 2.3: A schematic showing the microstructures that can in principle be generated during the isothermal transformation of austenite [6].

place at already existing grain boundaries, precipitates and defects [11]. If further growth of ferrite would result in an overall decrease in Gibbs free energy within the system, the ferrite nuclei is said to be stable and will grow [11]. Growth is achieved via long range diffusion, as the solubility of carbon is significantly lower in ferrite than in austenite. The solubility of carbon in ferrite reaches a maximum of 0.025 wt% at 727°C, whereas in austenite a maximum of 2 wt% at 1147°C can be achieved [12]. This can also be seen from the iron-carbon equilibrium phase diagram in Figure 2.2. Therefore, most of the carbon atoms have to diffuse out of ferrite into the surrounding austenite during transformation. Other alloying elements, such as manganese and silicon, also tend to migrate according to their equilibrium concentrations in ferrite and austenite. However, these elements have a significantly lower diffusion rate than carbon and require extensive time at high temperatures in order to reach their equilibrium distribution [13, 14].

2.2.2 Austenite

Austenite is a phase that is stable at high temperatures, as can be seen in Figure 2.2. Depending on the alloy and applied heat treatment it can in some cases be stabilised to lower temperatures (e.g. room temperature) and it is then called ‘retained austenite’. It has a face-centered cubic (fcc) crystal structure as depicted in Figure 2.1b. Compared to the bcc crystal structure, the atoms in the fcc crystal structure are closer to each other and it has therefore a higher atomic density. Austenite formation also occurs via nucleation and growth. The temperature where austenite first starts to form during heating is referred to as the A_{c1} temperature. Upon further heating more and more austenite is formed, until all of the material has been austenitised. The temperature where 100% austenite is reached is called the A_{c3} temperature. These critical temperatures are dependent on the heating rate [15, 16]. When full equilibrium is considered, the A_{c1} and A_{c3} temperatures are referred to as A_1 and A_3 and can also be seen in Figure 2.2. Between the A_{c1} and A_{c3} temperatures there is a temperature range which is called the intercritical region. Within this region the material is only partially austenitised.

In the work of Speich et al. [13] it was shown that the formation of austenite from a ferrite/pearlite microstructure occurs in three stages. During the first stage, carbon enriched austenite is formed from pearlite. This stage occurs very rapidly and finishes when the pearlite dissolution is complete. It is followed by a second stage, where austenite grows into the ferrite grains. Austenite can grow either from the already formed austenite, or, after nucleation, from high energy locations like grain boundaries and corners [13, 17]. The austenite growth rate is dependent on the alloying elements. If only carbon is considered, a state of paraequilibrium is reached and the growth rate of austenite is controlled by the diffusion of carbon through the austenite. However, as the steel in the current study has a significant amount of manganese and silicon, it is likely that these elements have to be

taken into account.

In their work, Speich et al. [13] point out that manganese can be an important rate controlling factor for austenite growth. Manganese has a diffusion rate in ferrite which is almost three orders of magnitude higher than in austenite and it is assumed that the diffusion of manganese in ferrite is initially the rate controlling factor [13]. Diffusion of manganese occurs either through the ferrite or (much faster) via the ferrite grain boundaries [13]. As a result, the outer rim of the austenite grain has a higher concentration of manganese, which lowers the austenite decomposition temperature upon cooling. This directly leads to the third step of austenite formation, which is the final equilibration of ferrite and austenite, where alloying elements are fully distributing according to their equilibrium concentrations in either phase. The equilibration rate is now controlled by manganese diffusion in austenite. For practical applications, this equilibration is not reached during intercritical annealing, as extraordinary completion times were reported (2000 to 4000 hours) [13]. The effect of silicon is similar to that of manganese, with the difference that manganese diffuses to austenite and silicon diffuses to ferrite. The three austenite formation steps were later confirmed in the work of Wei et al. [14].

2.2.3 Cementite

Cementite (Fe_3C) is a carbide phase and thus contains a relatively high amount of carbon. It has an orthorhombic crystal structure and is an important phase in the pearlite and bainite microstructures. Cementite can be seen as white lamellae in the pearlite image and black lamellae in the bainite images of Figure 2.3.

2.2.4 Bainite

Bainite is a microstructure that forms in the region above and just below the martensite start temperature (M_s), typically in the range of 550°C to 250°C [6, 18]. It consists of a fine mixture of ferrite and carbide. The sub-units of ferrite are shaped either like three-dimensional plates or have a more needle-like shape, where the needles are also referred to as laths [1, 8]. These plates or laths are grouped together in a spike-like shape which is called a sheaf [1, 8]. The carbide consists of cementite and therefore this ferrite-cementite mixture was in the past often (falsely) identified as a special type of pearlite [1, 19]. The formation of cementite is caused by the fact that the solubility of carbon in the bcc bainitic ferrite structure is low (Section 2.2.1). Therefore, carbon has to diffuse out of ferrite and forms a carbon rich phase (cementite) next to bainitic ferrite. Bainite can be distinguished in two different variants: upper bainite and lower bainite. Both variants are shown in Figure 2.4. Upper bainite forms at the higher temperatures within the bainite transformation region, typically between 550°C and 400°C [6]. It consists of individual ferrite sub-units which are

separated by a layer of cementite. Lower bainite, on the other hand, experiences also cementite precipitation within the ferrite sub-units and the surrounding cementite layer is therefore thinner. Lower bainite forms at lower temperatures, which typically range from 400°C to 250°C [6]. The precipitation of cementite within the ferrite sub-unit is thought to be caused by the lower transformation temperatures, which greatly reduce the diffusion rate of carbon in ferrite. As the solubility of carbon in ferrite is low, an effective way of ‘removing’ carbon in the ferrite sub-units is precipitation within the ferrite sub-unit, as the carbon has to diffuse only a short distance. The energy of the system can therefore be lowered relatively quickly, as opposed to the long-range diffusion needed otherwise [8, 20].

For a more thorough understanding of bainite it is important to consider its transformation mechanism. Since the identification of the bainitic microstructure by Davenport and Bain in 1930 [21] its nature has been the topic of much debate. Even before its ‘discovery’ there were already some inconsistencies present. So described Hultgren [22] in 1926 the structure as “needles of troostite”, where troostite was the name given to all fine mixtures of ferrite and cementite. Davenport and Bain described it in their paper as “martensite-troostite” and also names like “intermediate transformation”, “dark etching constituent” and “acicular ferrite” were used to refer to bainite [8]. Bain’s colleagues at the United States Steel Corporation gradually started to call this microstructure bainite. However, it would take years for the scientific community to also start using this name, with books failing to mention it as bainite as late as 1947 [8]. With naming this structure, the difficulties had only just started. The exact transformation mechanism and kinetics would be the subject of a discussion that would last nearly a century and is still not resolved. Today, two main theories can be identified, each of which has its own supporting evidence and usefulness.

The *diffusive theory* focuses on bainite formation via diffusion. The bainitic ferrite and cementite are presumed to both grow simultaneously and the rate of bainite formation is limited by the diffusion rate of carbon from bainitic ferrite to austenite [23]. The growth rate of the bainite sub-units is greater in the edgewise direction as here diffusion can take place over a three dimensional area, as opposed to a two dimensional area at the rest of the sub-unit. Therefore, lengthening of the sub-units prevails over thickening, resulting in the observed laths or platelets. The diffusive theory is capable to predict the growth limits of both Widmanstätten and bainitic ferrite [24]. It is also able to make reasonable predictions about the growth kinetics of bainite [4, 25, 26]. However, this theory is limited by its inability to account for the effects that carbide-forming elements have on the bainite transformation. With the concept of solute drag an explanation might be provided, but this is still an area of uncertainty [27].

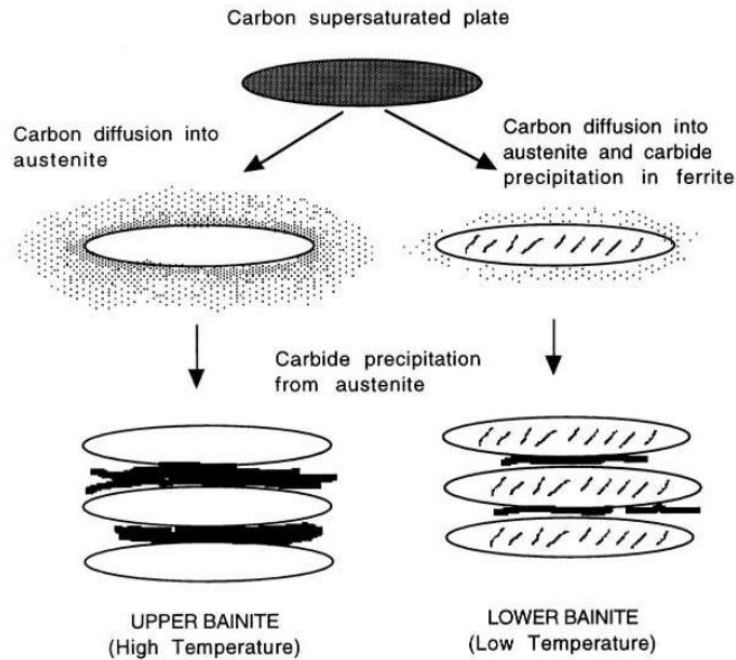


Figure 2.4: Schematic showing the differences between the formation of upper and lower bainite according to the diffusionless theory proposed by Bhadeshia [8].

According to the *diffusionless theory* a bainitic ferrite sub-unit is nucleated with the aid of carbon partitioning. This sub-unit then grows rapidly and diffusionless until the driving force for growth and the frictional force associated with plastic relaxation of the austenite matrix cancel out. Due to the diffusionless character of this mechanism the created sub-unit is supersaturated with carbon. Therefore, excess carbon is subsequently rejected into the surrounding austenite by diffusion, often followed by the precipitation of carbides. This process is schematically shown in Figure 2.4. When a new sub-unit nucleates, it nucleates near the tip of the previous sub-unit. This position is preferential as it can grow in a crystallographic orientation which is very similar to (or the same as) the ‘parent’ sub-unit. When nucleating at the side of the parent sub-unit it would have to take a crystallographic orientation that is different and which requires more energy [8]. Another advantage of nucleating near the tip is that the new sub-unit’s growth is less hindered by the layer of precipitated carbides (or enriched austenite) surrounding the ‘parent’ sub-unit [28]. The diffusion of carbon to the surrounding austenite enriches it in carbon. When no carbides precipitate, this enrichment can eventually become high enough to prematurely stop the bainite transformation. The reason for this is that the carbon enrichment lowers the driving force for subsequent nucleation and growth of a new sub-unit (it stabilises austenite). This event is also known as the incomplete reaction phenomenon (IRP) and results in a microstructure which only partially consists of bainite [1, 28, 29]. On further cooling, the remaining (carbon enriched) austenite typically decomposes partially into martensite. The diffusionless theory is able to explain the possible avoidance of upper and lower bainite in high and low carbon steels respectively [30]. It also explains why Widmanstätten ferrite can not

be formed in some steels and why other steels only transform to martensite [31]. In addition, it accounts for the lack of partitioning of substitutional solutes and is able to predict TTT and CCT diagrams with a reasonable accuracy [32]. The diffusionless theory has been used in industry for years and has resulted in the design of new bainitic alloys, heat treatments and microstructures with excellent properties, sometimes even exceeding those of other high-performance steel classes [33–35].

After having discussed both the diffusive and the diffusionless theory it is important to remember that one does not rule out the other. In the past, multiple scientists have argued that there might be a combined mechanism at work that incorporates both theories [36–40]. Vilella [36], for example, suggested that upper bainite was formed via a diffusion-controlled process, whereas lower bainite formed via lattice shearing (diffusionless process). Another example is the theory proposed by Speer et al. [37, 38], who suggested that a diffusionless mechanism may be responsible for the bainite transformation, but that the growth kinetics of the system are controlled by diffusion of carbon. The same idea was also proposed by Muddle and Nie [39] and Saha et al. [40].

2.3 Kinetics of Bainite Formation

The kinetics of a phase transformation are an important factor during the heat treatment of steel. They have a key role in determining at which temperature and at which rate a certain transformation occurs. In this section, available literature on the kinetics of bainite formation will be further reviewed. It is important to note that the formation of bainite is not yet fully understood and that multiple theories have been proposed by several authors to explain experimental observations.

2.3.1 Bainite Nucleation

Considering the kinetics of bainite formation, two distinct areas can be distinguished: nucleation and growth. During nucleation, the first cluster of atoms is adopting the new microstructure. Following classical nucleation theory this would normally be caused by random (thermal) vibrations in the system [8, 11]. However, as Bhadeshia points out [8], there is a linear relationship between the activation energy for nucleation and the driving force for bainite formation, where an inverse square relationship would be expected from classical theory. Bhadeshia explains this by stating that the nucleation of bainitic ferrite is not due to random fluctuations, but may instead be attributed to a “spontaneous dissociation of specific dislocation defects which are already present in the parent phase” [8]. When relating the activation energy for nucleation to the driving force for bainite formation, Bhadeshia also states that during bainite nucleation, the carbon is partitioned by diffusing out of the nucleus. This partitioning is needed in order to reduce the Gibbs free energy and to make the formation of the new phase possible. This would make the nucleus for Widmanstätten

ferrite and that of bainite the same, and, following the diffusionless theory, the applied growth mechanism will determine which of the two microstructures is formed [8]. Diffusional growth will result in Widmanstätten ferrite, whereas a diffusionless growth mechanism will result in bainite [8]. However, diffusionless growth requires more energy (driving force). This energy can be obtained by cooling the material to lower temperatures, as the driving force for transformation increases with decreasing temperature [11]. This would explain why the bainite transformation occurs at lower temperatures than the Widmanstätten ferrite transformation [6, 8].

2.3.2 Bainite Growth

Assuming diffusionless growth of bainite, carbon is only partitioned from bainite to austenite after bainite growth has occurred. Therefore, bainitic ferrite is initially supersaturated with carbon which increases its Gibbs free energy to a point where growth would normally be terminated. However, during growth, the surface-to-volume ratio decreases and thus the interfacial energy decreases. Following Bhadeshia [8], this decrease in interfacial energy would be high enough to sustain growth and the formation of supersaturated ferrite. Growth of a bainite sub-unit continues until the available driving force for growth and the frictional force caused by plastic relaxation of the austenite matrix cancel out. The growth rate of the individual bainite sheaves forms an important basis for discussion. According to the diffusionless theory [8] the growth can be divided into two parts. The growth of sub-units is diffusionless and is very fast. It is not as fast as the (also diffusionless) martensite transformation, as the growth of the sub-units would be severely reduced by the plastic work done to accommodate the sub-unit [8]. Additionally, the growth rate of the bainite sheaf also depends on the nucleation rate of successive sub-units. However, observations show that the growth rate of bainite is constant and not stepwise as would be expected from successive nucleation [41].

The requirements for bainite growth and the IRP are explained by the diffusionless theory with the aid of the T_0 theory [8]. This theory states that there only exists a driving force for the diffusionless growth of bainite at a certain transformation temperature if the Gibbs free energy of (bainitic) ferrite (G_{α_b}) is lower than the Gibbs free energy of austenite (G_γ). The diffusionless bainite growth stops when $G_{\alpha_b} \geq G_\gamma$. The temperature where G_{α_b} and G_γ are equal is given by the T_0 curve. It is important to note that G_γ decreases with the carbon enrichment of austenite, something that may occur during bainite formation. This may continuously lower the driving force for further bainite formation during the formation of bainite, until no driving force is left and the transformation comes to a halt (IRP). The T_0 theory does not include the contribution of non-chemical free energy, such as strain energy and interfacial energy, which is considered to be around 400 J/mol [8, 31]. Therefore, the T_0 curve was modified to include these energies and this modified version is known as the T'_0 curve [28, 42].

As mentioned before, there are theories that suggest that the growth of bainitic ferrite is fully diffusional [43]. In these theories bainite is often compared to pearlite, the main difference being that in pearlite the ferrite grows cooperatively with cementite, whereas it grows non-cooperatively in bainite. Following the diffusional theory, the growth rate would be limited by the diffusion of elements, such as carbon, across the different interfaces. This would indeed result in a more constant growth rate, but the observed growth rates are much higher than would be expected from the diffusion of carbon [8].

An important aspect in diffusional theories is the concept of solute drag. Substitutional (alloying) atoms are known to migrate to ferrite/austenite interfaces during the diffusional growth of ferrite. This segregation is said to have a “drag-like effect” on the movement of grain boundaries which may eventually stop the transformation (IRP) [44, 45]. However, it is also postulated that the IRP is not a general characteristic of bainite and is dependent on the involved alloying elements [44]. Besides the solute drag concept, diffusional theories often include a ledge-mechanism, where bainite grows in so-called ledges (something that might be seen as a form of non-lamellar pearlite growth) [46].

2.3.3 Bainite Formation Rate

To be able to say anything about bainite formation rates, it is important to look at the kinetics of bainite formation. These are dependent on two factors: the rate at which the nucleation of bainite starts and the rate at which new bainite sheaves form [47–49]. The initial nucleation of bainite is a heterogeneous process and starts along existing interfaces. These interfaces can be austenite grain boundaries, but also interfaces between two different phases, such as the ferrite/austenite interface [47–49]. After the initial nucleation, new bainitic sub-units nucleate at the newly formed bainitic ferrite/austenite interface. This process is autocatalytic and by subsequently forming new bainitic sub-units a bainite sheaf is formed. Both nucleation processes are schematically shown in Figure 2.5. The overall rate of bainite formation, df_{α_b}/dt , can be given as a function of the rate of initial bainite nucleation and the rate of the autocatalytic nucleation process. Using the same approach as in [48], df_{α_b}/dt can be stated as

$$\frac{df_{\alpha_b}}{dt} = \kappa_p \left[\exp\left(\frac{-Q_G^*}{kT}\right) + \exp\left(\frac{-Q_A^*}{kT}\right) f_{\alpha_b} \right] \quad (2.1)$$

where Q_G^* is the activation energy for initial bainite nucleation at the existing interfaces and Q_A^* is the activation energy for autocatalytic bainite nucleation at the bainitic ferrite/austenite interfaces. T is the bainite formation temperature and f_{α_b} is the current bainite fraction. The pre-exponential

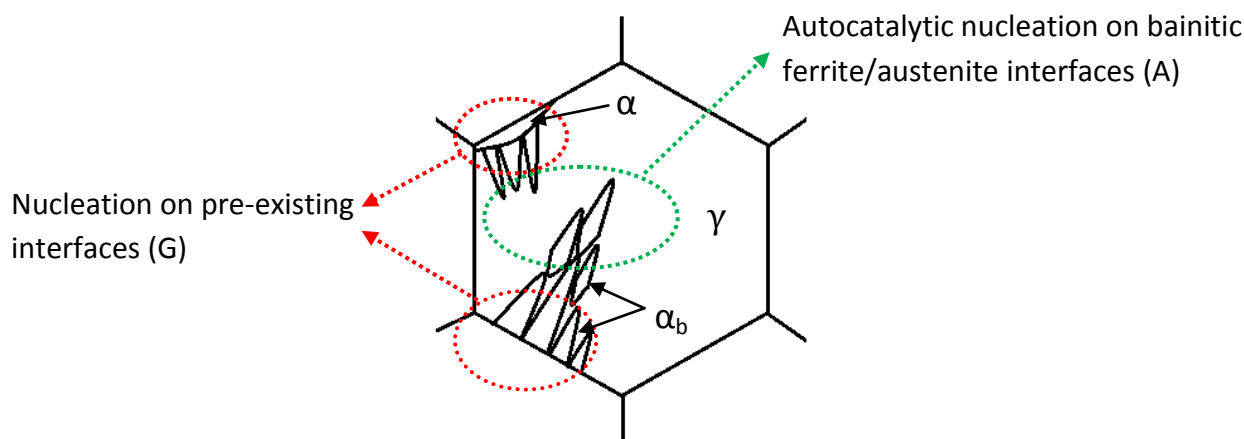


Figure 2.5: Schematic representation of an austenite grain with bainite growth, showing nucleation on pre-existing interfaces (austenite/austenite and ferrite/austenite) and autocatalytic nucleation of bainite.

In the figure, α denotes ferrite, α_b denotes bainite and γ denotes austenite.

factor κ_p is proportional to the number density of initial bainite nucleation sites at the existing interfaces N , as

$$\kappa_p \propto \frac{kT}{h} N \quad (2.2)$$

where k is the Boltzmann constant and h is the Planck constant. It is important to note that Equation 2.1 is proposed by Ravi et al. [48] under the assumption of a diffusionless bainite transformation mechanism. Although it matches experimental results rather well, its applicability to a diffusional point of view requires further study.

2.3.4 The Effect of Common Alloying Elements

Steel consists of a combination of iron and alloying elements. Iron is the element that makes up the crystal structure, but the alloying elements added to modern steels have a significant influence on the transformation of the crystal structure from one form to another. When dealing with the kinetics of bainite formation it is therefore important to include the effect of these elements. It has been found that increasing the total alloy content decreases the overall transformation rate (as austenite is stabilised) [8].

Carbon (C) is the prime alloying element in steel. Carbon plays an important role in bainite formation as it forms cementite, which precipitates around and (for lower bainite) inside the bainitic sub-units. As carbon diffuses out of bainitic ferrite it also increases the carbon content of the surrounding austenite, if cementite precipitation does not occur. This stabilises the austenite and

slows down the nucleation of new bainitic sub-units. This may result in a termination of bainite formation (IRP). Additionally, the stabilisation of austenite suppresses martensite formation, which might leave the material with a relatively high fraction of residual (retained) austenite after quenching. The total carbon content of the steel also has an influence on the type of bainite that is formed. Research on plain carbon steels shows that no lower bainite can be formed at all for carbon contents below 0.35 wt% [1, 50]. It is also reported that an increase in carbon content reduces the sheaf growth rate and results in plates with a smaller width [8].

Another alloying element is silicon (Si). This element has an extremely low solubility in cementite [8, 43]. Therefore, silicon retards the kinetics of cementite formation and in sufficient quantities (>1.5 wt%) it can even prevent cementite from forming at all [4, 51]. In the latter case, bainite consists only of bainitic ferrite and carbon-enriched austenite and is often referred to as carbide-free bainite [4, 8, 51]. Within carbide-free bainite, there are no cementite precipitates that can act as effective carbon-sinks. This means that the austenite becomes enriched in carbon, thus stabilising it. This can result in the IRP and as the M_s temperature also drops, a part of the austenite is often retained to ambient temperature. Silicon is more soluble in ferrite than in austenite, which gives it also ferrite-stabilising properties [52].

Manganese (Mn) is an element that is often used to improve the hardenability of steel. During the bainite transformation, Mn stabilises the austenite and is able to slow down the overall transformation rate [53, 54].

2.4 The Effect of Ferrite on Bainite Formation

To achieve an acceleration of bainite formation kinetics without altering the overall steel composition, one could try to increase the number density of preferential nucleation sites for bainite N , as stated in Equation 2.1. By doing this, bainite has more locations from where it can easily nucleate and grow from, resulting in a decrease in the time needed to form a certain fraction of bainite. One way to increase the number density of preferential nucleation sites is to form a small fraction of a different phase prior to the bainite transformation. Several studies have explored the effects of partial martensite formation prior to the bainite transformation [18, 55–59]. Indeed, these studies suggest that an acceleration of the bainite kinetics can be achieved. However, the different phase could just as well be ferrite. The effect of ferrite on the bainite transformation kinetics has in the past been studied by a only few authors. Quidort and Brechet [4] used a small amount of ferrite (<10%) in their study to trigger the bainite transformation in several 0.5 wt% C steels. They observed an accelerating effect on the bainite kinetics and ascribed this to the increase of preferential nucleation sites. In a more recent study, Zhu et al. [5] studied the effect that ferrite had on the bainite and

martensite transformations. They observed that a certain amount of ferrite (up to 51%) could also slow down the bainite transformation. They explain this contradiction with the observation that the ferrite/austenite interface contains a higher concentration carbon and manganese, which delays bainite formation. When this alloying concentration at the interface gets too high, it surpasses the accelerating effect of the ferrite interface itself and the bainite transformation is slowed down instead of accelerated.

In the work by Ravi et al. [3], the effect of an intermediate annealing treatment between full austenitisation and bainite formation on the bainite formation kinetics was studied. An Fe-0.2C-3Mn-2Si (wt%) steel was austenitised at 1000°C and then cooled down to intermediate temperatures of either 800°C or 600°C. After holding the material at this temperature for 1 to 30 minutes it was further cooled down to 400°C, at which temperature it was isothermally held and bainite was formed. Ferrite formation was observed during the annealing treatments at 600°C for annealing times longer than 10 minutes. For the other annealing treatments no ferrite formation was observed. The bainite formation kinetics of all the heat treatments that included annealing treatments at intermediate temperatures were compared to those of bainite formation without the intermediate annealing step. It was observed that all of the annealing experiments displayed a significant accelerating effect on the subsequent bainite formation kinetics.

To explain these findings, Ravi et al. [3] postulate that two different mechanisms are at work. When an observable fraction of ferrite is formed during the intermediate annealing step, the formed ferrite grains act as preferential nucleation sites for bainite. This increases the total amount of nucleation sites N , and thus accelerates the transformation. However, when the ferrite fraction becomes larger, the carbon content of the remaining austenite increases as the bcc ferrite structure leaves little room to accommodate carbon. The increased carbon concentration stabilises the austenite, decreasing the driving force for bainite nucleation. Larger fractions of ferrite can therefore have a retarding effect on the formation of bainite. These findings agree with the work of Quidort and Brechet [4] and Zhu et al. [5].

In the cases where no ferrite formation was observed during annealing, an acceleration of subsequent bainite formation was still observed. Ravi et al. [3] therefore proposed a second mechanism. During annealing, solute (in this case mainly carbon due to its relatively high diffusion rate) segregates to the austenite grain boundaries. This increases the solute concentration at the austenite grain boundaries, but also creates areas in the vicinity of the austenite grain boundaries which are depleted in solute. These depleted areas are favourable nucleation spots for ferrite. Although they were not observed in their study, Ravi et al. theorise that ferrite nuclei are in fact present when the material is subjected to an intermediate annealing treatment. While ferrite growth was thermodynamically

possible, these nuclei did not grow to ferrite grains that could be observed. This could be ascribed to kinetic reasons. This means that for higher annealing temperatures (lower driving force for transformation) or shorter annealing times the ferrite nuclei form, but do not grow. These ferrite nuclei become important during the bainite transformation, as these already have the bcc structure needed to form bainite. Therefore, bainite does not have to nucleate, but can grow from the existing bcc (ferrite) nuclei as soon as the temperature is dropped. This results in increased transformation rates and thus gives the second mechanism proposed by Ravi et al. to be at work during bainite formation.

In the current study the effect of ferrite on the bainite transformation kinetics is further studied. The ferrite fractions are varied to a maximum of 25% and the subsequent formation of bainite is compared to bainite formation without prior ferrite formation. Ferrite can be obtained in different ways. If the material is fully austenitised, ferrite can be formed by keeping the material for a sufficiently long time at a sufficiently high temperature. This can be achieved by an isothermal hold at intermediate temperatures (as in the work of Ravi et al. [3]) or by application of a slow cooling rate. Another way to obtain a certain ferrite fraction is intercritical annealing, where the material is heated to a temperature in the intercritical region (between the A_{c1} and A_{c3} temperatures). Within this region the material is only partially austenitised and part of the original ferrite content (if present) can in this way be retained. In the current work both slow cooling and intercritical annealing are utilised to produce a certain ferrite fraction and its effects on the subsequent formation of bainite are studied. Especially ferrite retention through intercritical annealing would make it possible to adjust the bainite formation kinetics, without the need for an additional annealing treatment to form ferrite. This study will be focused on the bainite formation kinetics in the presence of ferrite and the effect of different ferrite fractions and morphologies. From a scientific point of view, the results will lead to an improved understanding of the bainite formation kinetics in the presence of ferrite. From an industrial point of view, the outcome of this study may lead to more efficient heat treatments that result in a higher production output and may also influence future alloy design.

Chapter 3: Experimental Methods

In this chapter the experimental methods will be discussed. This includes the material used and the steps that were taken to prepare the samples. The different heat treatments that were applied, equipment that was used to study the samples and the analysis methods used will also be elaborated.

3.1 Material

Steel with a nominal composition of Fe-0.2C-3Mn-2Si (wt%) is used in this study. The material was cast and hot-rolled to a slab with dimensions of 485 x 120 x 6.2 mm³. From this slab, dilatometer samples were manufactured. These samples had a solid cylindrical shape with a length of 10 mm and a diameter of 4 mm. The samples were cut out of the slab using electrical discharge machining (EDM), where the length of the cylindrical samples was aligned with the rolling direction of the slab. To prevent any edge-effects, the edges, ends and surfaces of the slab were not included in any of the samples. In Appendix A an overview is given of the sample locations and dimensions.

The initial microstructure of the samples consists of a fine pearlitic matrix with blocks of ferrite and bainitic areas (see Figure 3.1). It was also observed that the initial microstructure shows considerable banding, due to the segregation of alloying elements during solidification. These bands are clearly visible in Figure 3.2, where the light bands mainly consist of ferrite and the dark bands mainly consist of pearlite and bainite.

3.2 Dilatometry

When researching solid-state phase transformations in steel, dilatometry is one of the most important tools available. Not only can it apply the desired heat treatment, but it also allows for in-situ observation with respect to the dimensional (length) changes of the sample. As explained in Section 2.2, when the material transforms from one phase to another, the crystal structure changes. Each crystal structure has its own atomic packing density. The bcc structure has a relatively low density and the fcc structure has a higher density. When the material is heated above a certain temperature (A_{c1}), bcc transforms to fcc. This is accompanied with a decrease in sample dimensions, as the

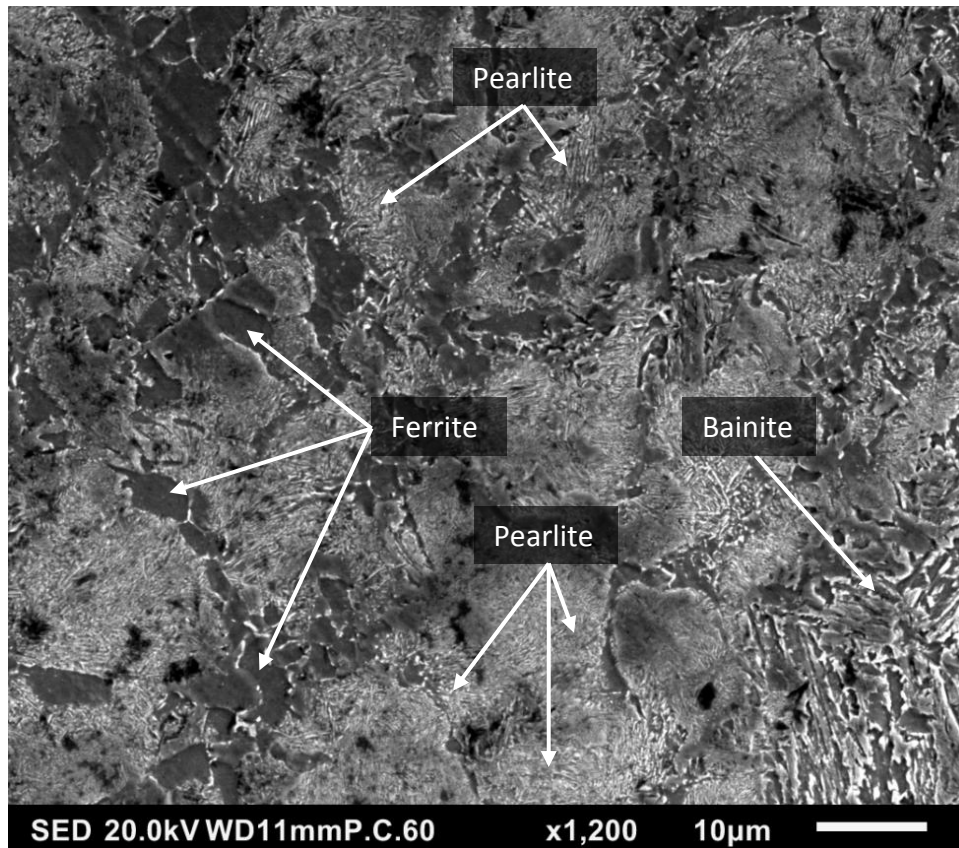


Figure 3.1: SEM image of the initial microstructure.

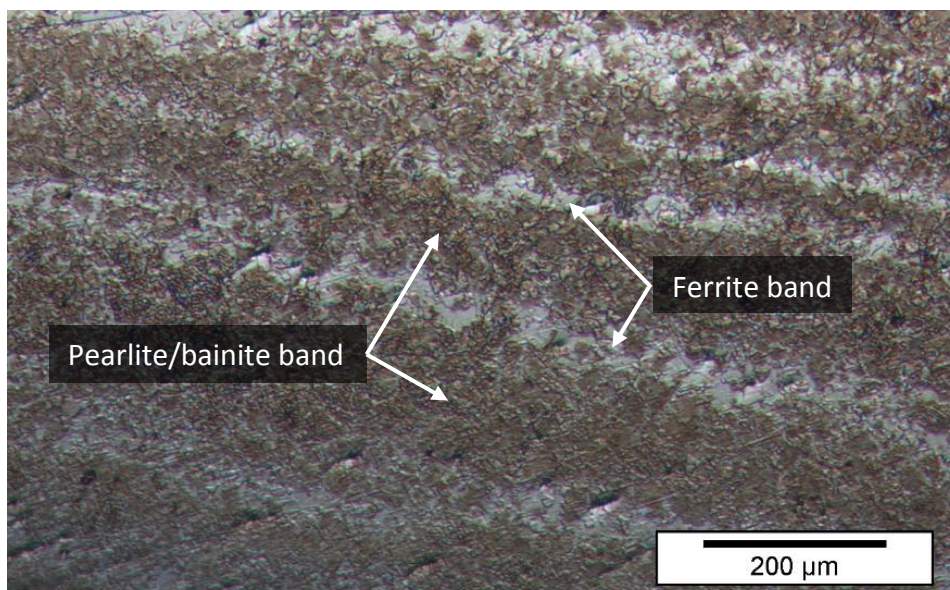


Figure 3.2: Light optical microscopy image of the initial microstructure. Banding is clearly visible, with ferrite bands in light grey and pearlite/bainite bands in dark brown.

volume occupied by the atoms decreases. This phenomenon can be seen in the dilatometry curves, of which an example is shown in Figure 3.3.

Increasing the temperature of a steel sample will result in thermal expansion of the sample [60]. However, at a certain point the expansion will come to a halt and changes to a contraction of the sample instead, as shown in Figure 3.3. The point where this change occurs is identified as the A_{c1} temperature: the start of the transformation from the bcc to the fcc crystal structure. With further heating, the sample will become more and more austenitic (fcc). When most of the bcc phase is transformed to the fcc phase the sample dimensions will gradually stop decreasing and start increasing again, eventually following the thermal expansion curve again. This point is identified as the A_{c3} temperature (see Figure 3.3). Due to the change to fcc, the curve will now have a different slope, as the thermal expansion of the fcc structure is different from the bcc structure [60]. The same principle can be applied to other phase transformations anywhere during the heat treatment. Thus, keeping track of the dimensional changes is of great significance, as the expansion or contraction of the sample provides information about the phase transformation taking place.

3.2.1 Critical Temperatures and the Lever Rule

To identify the A_{c1} and A_{c3} temperatures from a full austenitisation expansion curve, two linear lines are fitted through the data (red lines in Figure 3.3). These lines represent the thermal expansion of the bcc and fcc phases, respectively, as the exponential relationship described by Van Bohemen [60] approaches linearity at high temperatures. The A_{c1} and A_{c3} temperatures can then be found by determination of the point where the experimental data starts to become highly non-linear. When these temperatures are found, they can be used to obtain an estimate of the austenite fraction that has formed at a particular intercritical temperature. To do this, the lever rule is applied. Using Figure 3.3, the lever rule is given by

$$f_{\gamma} = \frac{AX(T)}{AB(T)} \quad (3.1)$$

where the fraction of austenite at a certain temperature, f_{γ} , is given as a function of the difference between the experimental curve and the bcc expansion curve, $AX(T)$, and the difference between the fcc and bcc expansion curves, $AB(T)$.

3.2.2 Martensite Start Temperature

When the material that is used in this study is quickly cooled from a temperature above M_s to room temperature, it forms martensite. M_s denotes the martensite start temperature, the temperature

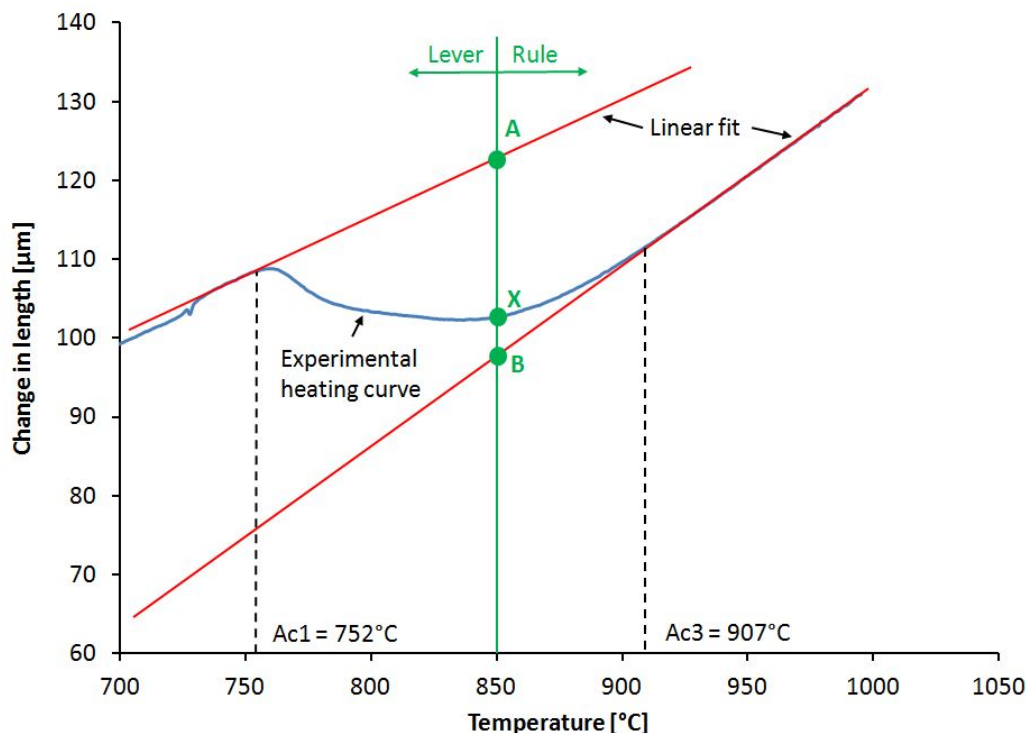


Figure 3.3: Dilatometric curve showing the determination of the A_{c1} and A_{c3} temperatures and the application of the lever rule.

where martensite starts to form during cooling. This temperature is determined by fitting a linear curve to the expansion data during cooling, similar to the determination of the A_{c1} and A_{c3} temperatures. This is shown by the red line in Figure 3.4. At the temperature where martensite starts to form, the experimental expansion curve starts to show expansion in addition to the contraction resulting from cooling, as fcc austenite is transformed to martensite with a bcc-like structure. M_s is in this work defined as the temperature where the experimental expansion data is $0.5 \mu\text{m}$ larger (less negative/more positive) than the linear curve. This criterion was chosen as fluctuations in dilatometry data around the true expansion of the sample were smaller than $0.5 \mu\text{m}$ and thus a deviation from this limit would indicate a phase transformation (in this case the formation of martensite).

3.2.3 Equipment

The dilatometer used in this study is the Bähr DIL 805 A/D [61]. This is a push-rod quench dilatometer, which keeps the sample suspended in mid-air by gently pushing two quartz rods on the sample ends (rods A and B in Figure 3.5). The applied force is only just enough to keep the sample suspended and will not noticeably hinder/aid the sample's expansion/contraction. A third quartz rod (rod C in Figure 3.5) is located parallel to the quartz rods that hold the sample. This quartz rod acts as a reference to which thermal expansion of the sample is measured. The thermal expansion of the quartz rods is accurately known and embedded in the dilatometry software. By measuring the

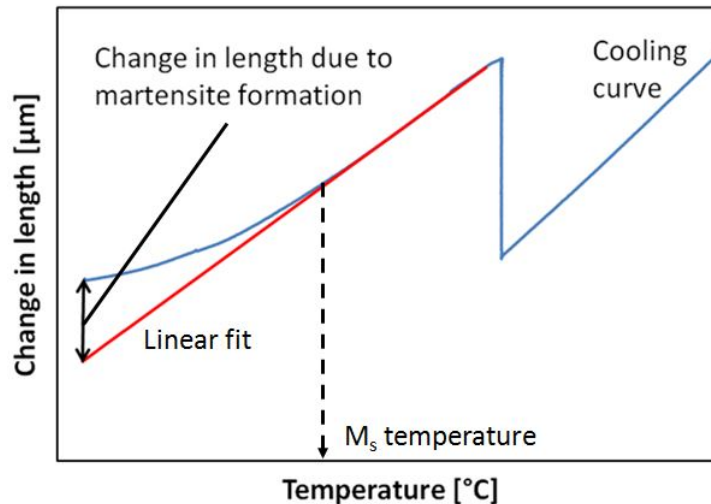


Figure 3.4: Change in length due to the formation of martensite.

difference in expansion between rod A + sample + rod B and rod C the expansion of the sample without the effect of the expanding equipment around it can be calculated (as the surrounding equipment is exactly the same for rod A + rod B and rod C). Rods B and C are connected to a Linear Variable Differential Transformer (LVDT), which is a sensor that measures linear changes in length with a resolution of 50 nm. The sample is heated using an induction coil. This coil consists of a hollow tube, which is perforated at the inside. Temperature is regulated by the accompanying software in combination with an S-type thermocouple spot welded onto the sample's surface. For cooling, helium gas is used. The gas travels through the perforated tube structure of the induction coil and, escaping from the holes, cools the sample from all radial directions. This allows for high cooling rates, making this dilatometer also suitable for quenching experiments. With the Bähr DIL 805 A/D, heating rates of 100°C/s and controlled cooling rates of up to 100°C/s can be achieved [61]. During quenching the maximum cooling capacity of the dilatometer can be used to quickly cool the samples. This involves a maximum flow of helium cooling gas and quenching rates of over 300°C/s were obtained in this study.

3.3 Heat Treatments

To form a certain fraction of ferrite before the bainite transformation, intercritical annealing is used (see also Section 2.4). The material is heated to a temperature between the A_{c1} and A_{c3} temperatures, where the material is only partially austenitised. This way, part of the original phase composition continues to exist aside from the newly formed austenite. In Section 3.1 it was shown that the initial microstructure consists of ferrite, pearlite and bainite. The carbides in pearlite and bainite will dissolve in the first stage of austenite formation [13, 62], which leaves only ferrite and austenite after the first stage. Thus, by choosing a range of intercritical temperatures closer to the

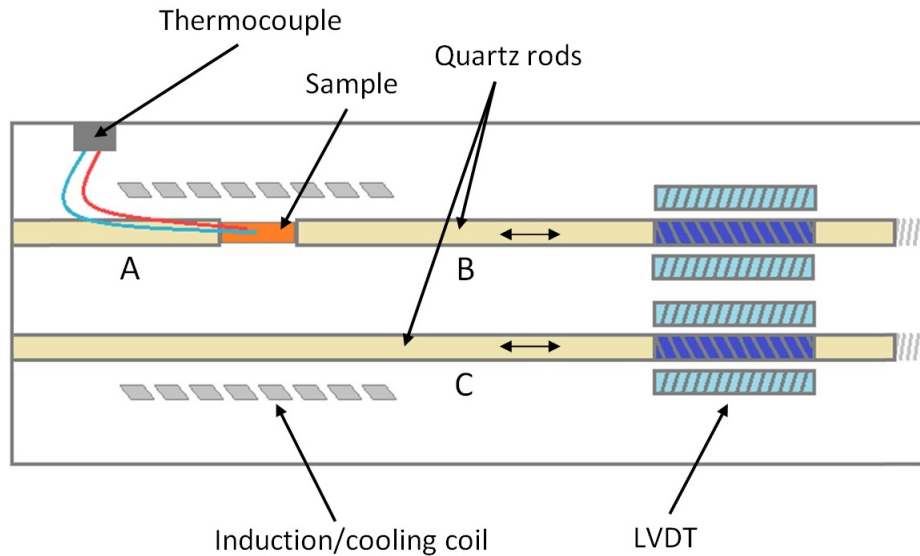


Figure 3.5: Schematic showing different parts within the Bahr DIL 805 A/D dilatometer.

A_{c3} than the A_{c1} temperature, the material should consist of ferrite and austenite only.

The first set of heat treatments that was applied served to gather important data about the material. These heat treatments consisted of heating to 1000°C , whereafter the sample was quenched with helium gas. As research by various authors has shown that the A_{c1} and A_{c3} temperatures are dependent on the heating rate [15, 16], these full austenitisation heat treatments were carried out for all three heating rates of 1°C/s , 5°C/s and 10°C/s . From these experiments the A_{c1} and A_{c3} temperatures could be determined for each heating rate.

After the critical temperatures had been determined, three types of heat treatments were applied, denoted by HT-1c, HT-2c and HT-3c. The first two types of heat treatments can be found in Figure 3.6 and Figure 3.7 and differ in heating rate and top temperatures only. Intercritical annealing involved holding the sample at the desired intercritical temperature for 180 seconds, after which it was cooled under vacuum with a rate of 2°C/s during which ferrite could be formed. After cooling to a bainite formation temperature of 400°C , the sample was retained at this temperature for 1500 seconds and subsequently quenched.

The third type of heat treatment applied in this study is referred to as HT-3c and is shown in Figure 3.8. This heat treatment takes a different approach at retaining a certain ferrite fraction. It includes a slow heating rate of 1°C/s to ensure a uniform temperature within the sample. This heat treatment does not include an intercritical isothermal hold and the sample is directly cooled with 30°C/s using helium gas as coolant. The bainite formation temperature was again set at 400°C , but a slightly longer holding time of 1800 seconds was used.

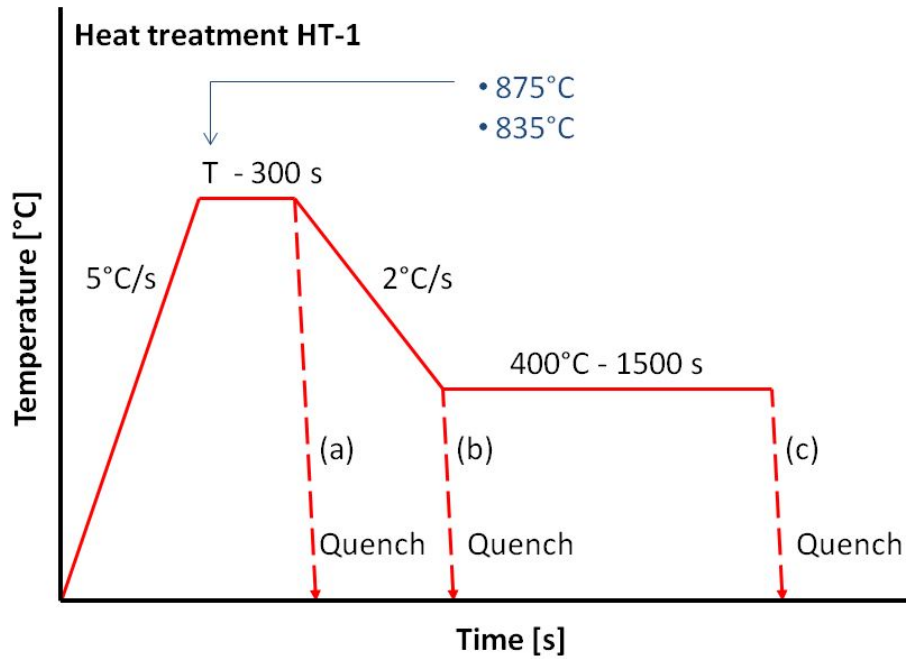


Figure 3.6: Schematic showing the heat treatments with a heating rate of 5°C/s .

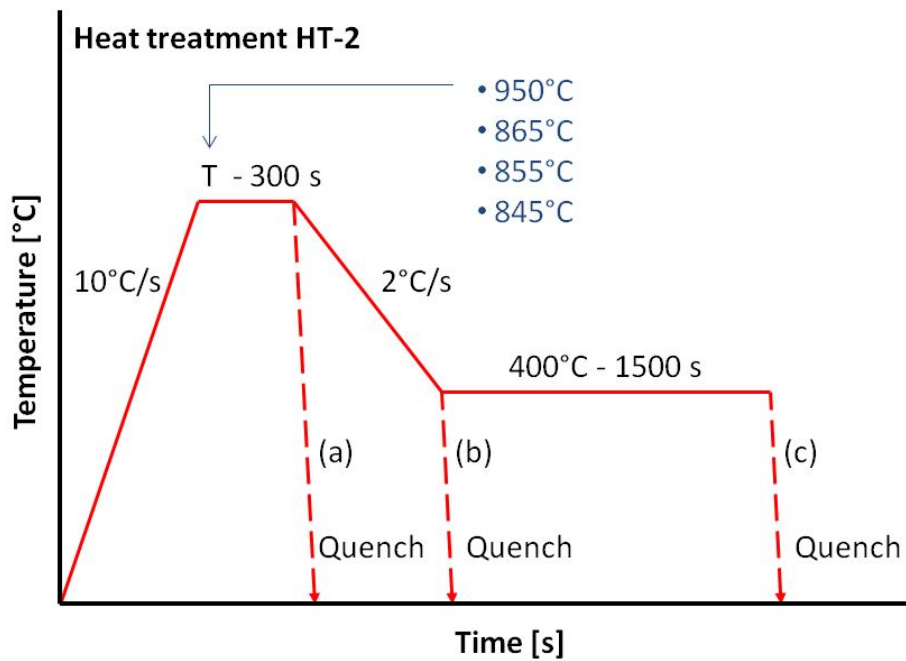


Figure 3.7: Schematic showing the heat treatments with a heating rate of 10°C/s .

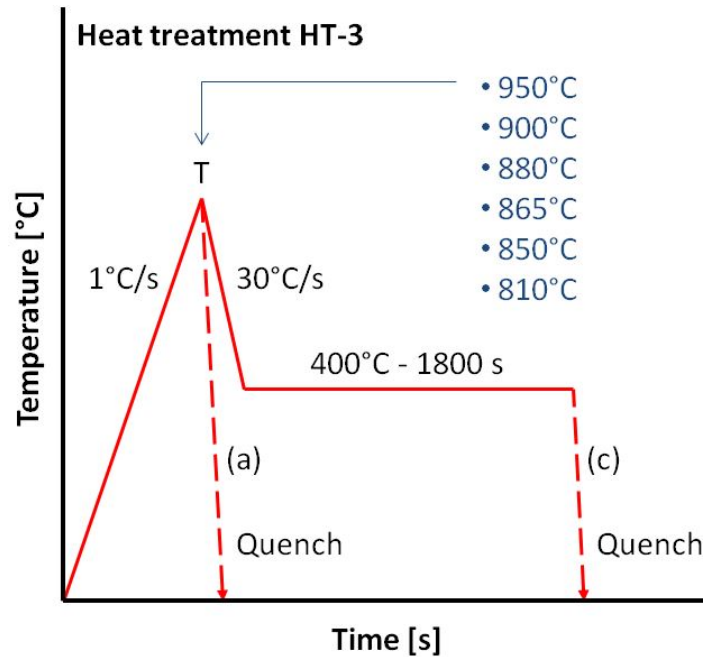


Figure 3.8: Schematic showing the heat treatments which omit the intercritical isothermal hold and apply fast cooling.

Aside from the heat treatments where bainite is formed (HT-1c, HT-2c and HT-3c), additional quench experiments were carried out, which are indicated by the letters 'a' and 'b' (as can be seen in Figures 3.6, 3.7 and 3.8). These experiments serve to capture the microstructure at certain points along the heat treatment route and are used to study the ferrite fraction and morphology at these points. Quenching rates as high as 96°C/s were achieved when quenched from 400°C . Quenching from intercritical temperatures achieved even higher quenching rates of 310°C/s .

3.4 Metallographic Preparation

Before microstructural information can be obtained by optical microscopy and scanning electron microscopy, a proper preparation of the samples is required. The cylindrical dilatometry samples were fitted into a simple tool, in which they could be clamped and adjusted in height (see Figure 3.9). The sample surface was then sanded and polished using the steps indicated in Table 3.1, with a final polish consisting of $1\ \mu\text{m}$ sized particles. During sanding it was made sure that at least 2 mm of material were removed, to avoid any edge effects that might be there as a result of the dilatometer quartz rods. The final result is a sample with a length of approximately 7 mm, a diameter of 4 mm and a neatly flat and polished surface on one end of the cylindrical sample.



Figure 3.9: Tool used to hold samples during metallographic preparation.

Table 3.1: Grit and particle sizes used during the sanding and polishing stages of metallographic preparation

Grit	80	180	320	800	1200	2000	3 μm	1 μm
Material	SiC	SiC	SiC	SiC	SiC	SiC	diamond suspension	diamond suspension

To reveal the microstructure itself, the samples were etched with a 2% nital solution (2% nitric acid and 98% alcohol). This etchant nicely revealed the different phases and, especially during scanning electron microscopy, the ferrite/bainite structures could clearly be seen. Etching times ranged from 2 to 6 seconds, depending on the specific heat treatment.

3.5 Optical Microscopy

Light optical microscopy was carried out using a Leica DMLM optical microscope with ColorView soft imaging system in combination with AnalySIS Auto software. Magnifications ranged from 50x to 500x.

3.6 Scanning Electron Microscopy

Since the heat treatments lead to highly refined microstructures, an imaging method was required that provided both high magnifications and high resolutions. The solution was found in scanning electron microscopy (SEM) using secondary electron imaging (SEI). For this a Jeol JSM-IT100 SEM was used. Detailed grey-tone images at magnifications in the range of 400x up to 3000x were obtained this way.

SEI uses the secondary electrons to create a grey-tone image. Secondary electrons are created when the electrons of the incident primary electron beam interact in an inelastic manner with the electrons from the sample's atoms. The incident electrons provide enough energy to eject the electrons from the outer bands, usually the valence or conduction bands, as the electrons in these bands do not require much energy to be ejected. These ejected electrons are called secondary electrons and

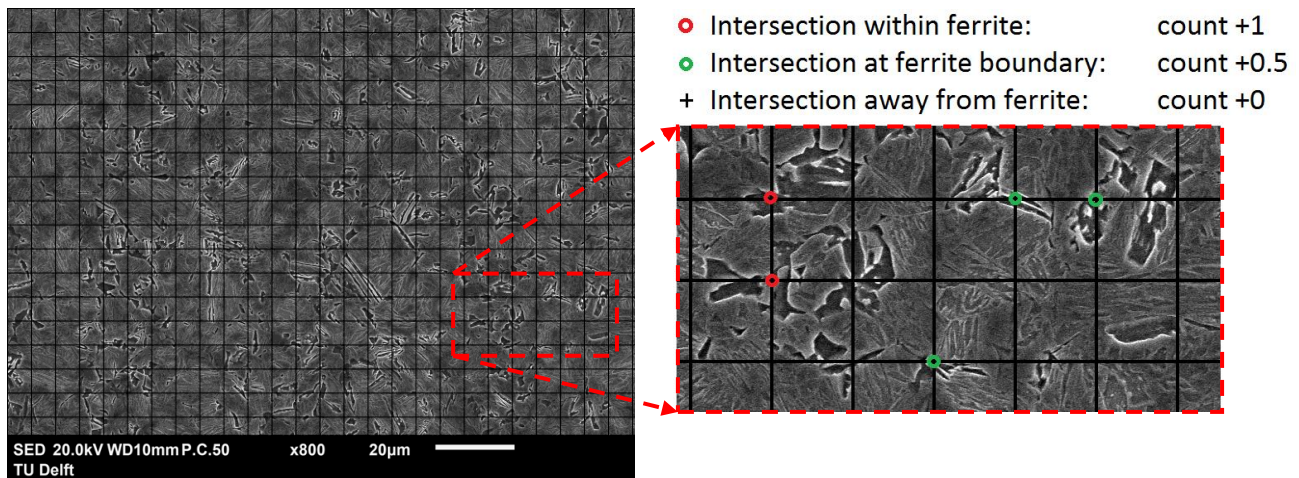


Figure 3.10: The image analysis method used in this study to determine the ferrite fractions, following ASTM standard E562 [63]

are now free to travel and leave the sample surface. They can also interact with neighbouring atoms and produce more secondary electrons. The image is formed using a secondary electron detector. This detector attracts the slow moving secondary electrons by using a positively charged field (in the range of +400 V). The secondary electrons are then further accelerated by a second positive charge (around +2000 V). This gives the electrons enough energy to emit flashes of light when they hit the actual detector (cathodoluminescence) which are then turned into an electric signal and further processed to form an image. As only the secondary electrons emitted by atoms near the sample surface are able to escape the material, SEI can be used to study the surface topology of a sample. When the sample consists of an etched metallic specimen it can therefore also provide microstructural information.

Throughout this study, image analysis is frequently used to estimate phase fractions. For this, the Systematic Manual Point Count technique was used, as described by ASTM standard E562 [63]. This technique consists of applying a square grid over the SEM image, after which the grid intersections are visually checked (an example is given in Figure 3.10). When the intersections are inside a grain of which the fraction is to be determined, they are counted as one. If the intersection is located at the boundary of the grain, they are counted as a half. In all other cases the grid intersection is counted as zero. In the end, all the counts are summed and divided by the total number of grid intersections, thus giving an estimate of the phase fraction. For this method, SEM images with a magnification of 800x were used, resulting in an image area of 159 x 108 µm. The grid consists of 25 x 17 evenly spaced lines (not counting the outer borders) which results in a total of 425 intersections. For each sample this was done for 3 to 5 images, after which the fraction average

of the different images was assumed to be closest to the real fraction.

3.7 Micro-Hardness Testing

Micro-hardness tests were performed using a Struers DuraScan 70 equipped with a Vickers micro-hardness indenter. A force of 0.5 kgf was used to create the indentations. The data was analysed using Ecos Workflow software. Indentation diagonals in the range of 44 μm to 52 μm were measured. As the material does not have a homogeneous microstructure, it was decided to perform 16 individual measurements on each sample. These points were arranged in a 4 x 4 square grid, where the gridlines were spaced 0.5 mm apart. According to ASTM standard E384 [64] the distance between the individual points is more than enough to assume that the measured points are not influenced by neighbouring measurements (the standard states this to be true when the distance between the points is larger than 2.5 times the indentation diagonal). After the 16 measurements had been performed, the average was used to provide an estimate of the overall hardness value of the sample. To perform the hardness tests, the optical microscopy samples were repolished to remove any etching. This resulted in flat and parallel surfaces.

Micro-hardness tests were chosen as they offer a non-destructive way to analyse the hardness of small samples. The hardness values serve as a first indication of the effect that the different heat treatments have on the mechanical properties of the material.

Chapter 4: Results and Discussion

In this section of the thesis the results will be shown and discussed in detail. It will start with presenting the ferrite fractions, their morphology and the effect of prior ferrite on the surrounding austenite. It is followed by the formation of bainite and the effects of ferrite on the formation of bainite are discussed, including the transformation rate, bainite morphology and micro-hardness tests.

4.1 Critical Temperatures

The A_{c1} and A_{c3} temperatures have been identified for each of the three heating rates 1°C/s, 5°C/s and 10°C/s, using the method described in Section 3.2. The results are shown in Table 4.1. As can be seen the critical temperatures increase with increasing heating rate, something which is also found in the work of Caballero et al. [15], where it is proposed that this is a general phenomenon in steels.

The heating curves of all heat treatments in this study displayed considerable deviation. Some curves followed an approximately linear route until the A_{c1} temperature was reached. Others, however, started to curve downwards at temperatures between 500°C and 600°C. An example from heat treatment HT-3c is given in Figure 4.1, where the start of the deviation is indicated. De Cock et al. [65] ascribe this “dilatometric anomaly” to the recrystallisation and defect annihilation of cold rolled steel. However, the material in this study was hot rolled and the effects of recrystallisation and defect annihilation are therefore not expected to be that significant. A different explanation was found in the work of Wei et al. [14], who ascribe this deviation to the (early) growth of thin films of retained austenite, which were able to bypass the nucleation barrier (which is normally possible at

Table 4.1: A_{c1} and A_{c3} temperatures sorted by heating rate.

Heating rate	1°C/s	5°C/s	10°C/s
A_{c1} [°C]	728	756	760
A_{c3} [°C]	917	920	940

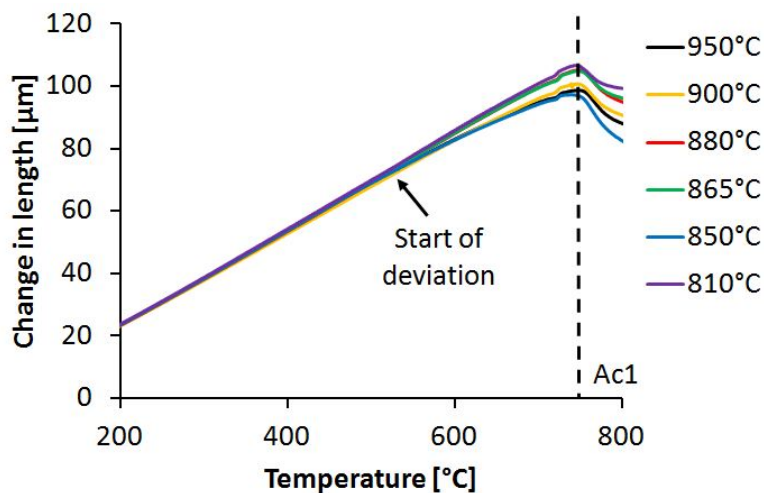


Figure 4.1: Dilatometric heating curves of heat treatment HT-3c.

temperatures $\geq A_{c1}$) as some retained austenite was already present. A_{c1} temperatures remained (approximately) constant for each heat treatment and ferrite fractions are therefore unlikely to be affected.

4.2 Prior Ferrite

Before the samples are heat treated, an estimate of the ferrite fractions can be made using the lever rule mentioned in Section 3.3, under the assumption that no cementite is left. This was done for each of the intercritical annealing temperatures (and heating rates) in heat treatments HT-1, HT-2 and HT-3. The results are shown in Figure 4.2a. As could be expected, higher annealing temperatures result in a smaller ferrite fraction. Figure 4.2a also shows a difference with respect to heating rate. This can be explained by the shift in critical temperatures with the change of heating rate (see Table 4.1).

4.2.1 Ferrite Fractions Before Cooling

In heat treatments HT-1 and HT-2 an isothermal hold of 300 seconds at the intercritical temperature precedes cooling down to 400°C. During this hold, a further contraction of the sample was observed indicating the continued formation of austenite. The intercritical isothermal hold provides extra time and austenite is therefore likely to continue to grow until equilibrium is reached.

The samples from heat treatments HT-1a and HT-2a were analysed with the image analysis method described in Section 3.6 and the ferrite fractions were determined. The results are given in Figures 4.2b and 4.2c. When the ferrite fractions of heat treatments HT-1a and HT-2a are compared to the fractions estimated by the lever rule, it can be seen that the remaining ferrite fraction decreased

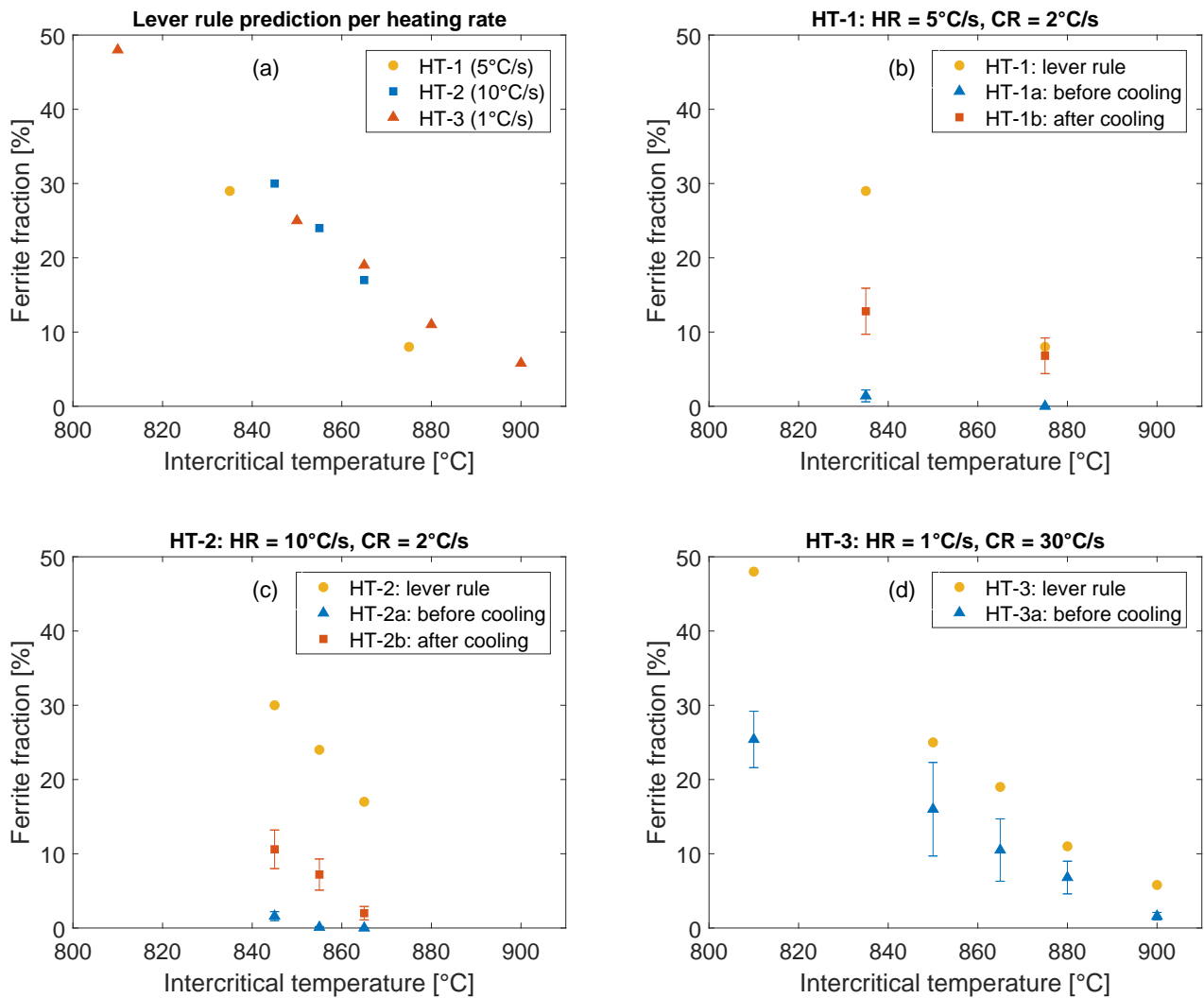


Figure 4.2: Different ferrite fractions as a function of the intercritical temperature used in the heat treatments, with (a) the fractions at the start of the intercritical isothermal hold as predicted by the lever rule, (b) the fractions concerning heat treatment HT-1, (c) the fractions concerning heat treatment HT-2 and (d) the fractions concerning heat treatment HT-3. HR and CR denote heating rate and cooling rate, respectively. Error bars provide the standard deviation between multiple metallographically analysed images (in some cases too small to be visible).

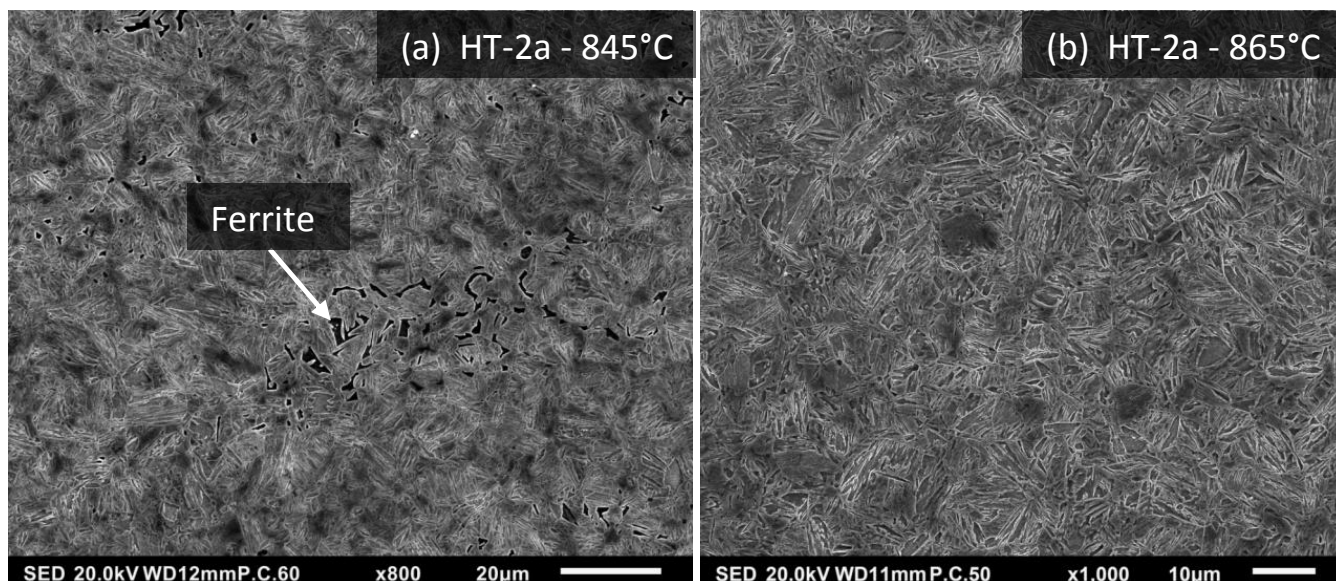


Figure 4.3: SEM images of heat treatment HT-2a with intercritical annealing temperatures of (a) 845°C and (b) 865°C. The microstructure consists of a mixture of martensite and austenite and in (a) also ferrite grains can be distinguished (dark).

considerably during the intercritical isothermal hold. It is clear that most of the ferrite has transformed to austenite, leaving only very minor fractions of ferrite. Figure 4.3 shows two SEM images from the samples that were quenched directly after the isothermal hold. In Figure 4.3a, a minor ferrite fraction is still visible, while in Figure 4.3b only the martensite/austenite matrix can be seen.

Heat treatment HT-3 uses a heating rate of 1°C/s, does not include an intercritical isothermal hold and the material is directly cooled to 400°C with a rate of 30°C/s. This results in more time for transformation during heating and allows little time for continued austenite formation after the desired intercritical temperature has been reached. Samples from heat treatment HT-3a (quenched after reaching top temperature) were analysed and the results are shown in Figure 4.2d. As can be seen from this figure, the obtained ferrite fractions are considerably higher than those in heat treatments HT-1a and HT-2a. However, the fractions are lower than those predicted by the lever rule. An explanation for this may be found in the carbon concentration of austenite, which decreases with increasing austenite fraction. The carbon concentration influences the lattice parameter in austenite and a lower carbon concentration will result in a smaller lattice parameter of austenite [66]. As the lever rule assumes constant lattice parameters, this introduces an error in the predicted ferrite fraction. This effect is also found in the work of Lee et al. [67], where similar differences between lever rule predictions and actual ferrite fractions moved the authors to look for an alternative way to predict ferrite fractions during intercritical annealing.

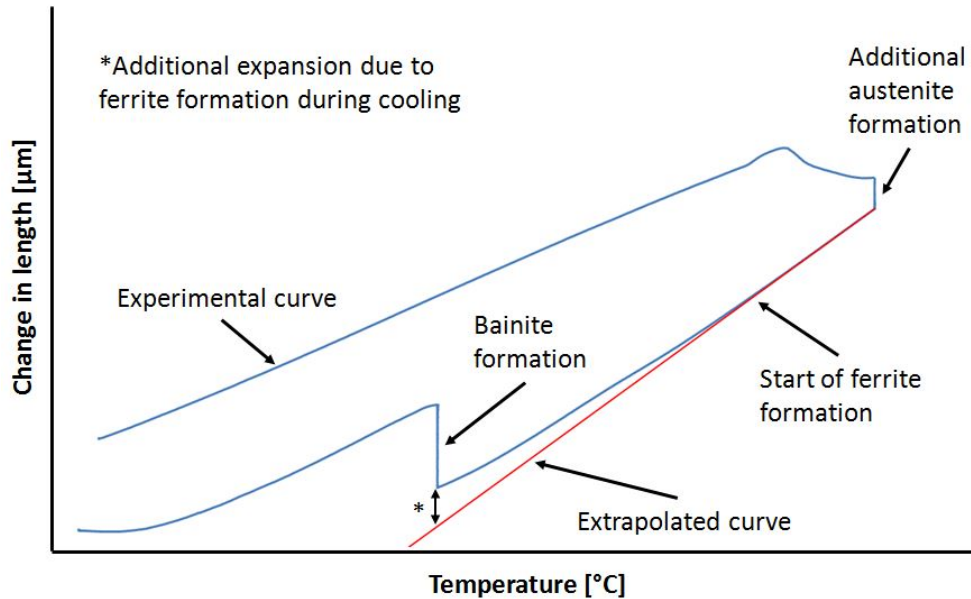


Figure 4.4: Dilatometric curve of heat treatment HT-2c, having an intercritical annealing temperature of 855°C. The onset of ferrite formation during cooling and the expansion due to ferrite formation have been outlined.

4.2.2 Ferrite Fractions After Cooling to 400°C

Heat treatments HT-1 and HT-2 use a cooling rate of 2°C/s to cool from intercritical temperature to 400°C. For the full austenitisation experiments, this cooling rate proved high enough to prevent any observable phase transformation during cooling. However, in addition to the contraction caused by the decrease in temperature, the dilatometric curves from heat treatments HT-1b, HT-1c, HT-2b and HT-2c show considerable expansion, as outlined in Figure 4.4. This indicates that an fcc to bcc phase transformation took place. By means of optical and scanning electron microscopy it was determined that the formed bcc phase was ferrite. From this, two things can be concluded. First of all, a cooling rate of 2°C/s is for this material not high enough to prevent phase transformations during cooling from intercritical temperatures. Secondly, during cooling to the bainite transformation temperature, the ferrite fraction was increased.

The observed phase transformation can be explained by looking at the annealing temperatures involved. During preliminary experiments, where cooling rates down to 1°C/s were used, no phase transformation occurred during cooling to 400°C. However, these experiments used annealing temperatures of 1000°C, which is well above the point of full austenitisation (see Table 4.1). For a phase transformation to occur during cooling, the new phase would have to both nucleate and grow. If, on the other hand, the annealing temperatures are decreased to the intercritical region, a fraction of ferrite will be left in the material. Therefore, ferrite does not have to nucleate and can grow from the existing ferrite grains. As nucleation takes time and subsequent growth requires an energy barrier

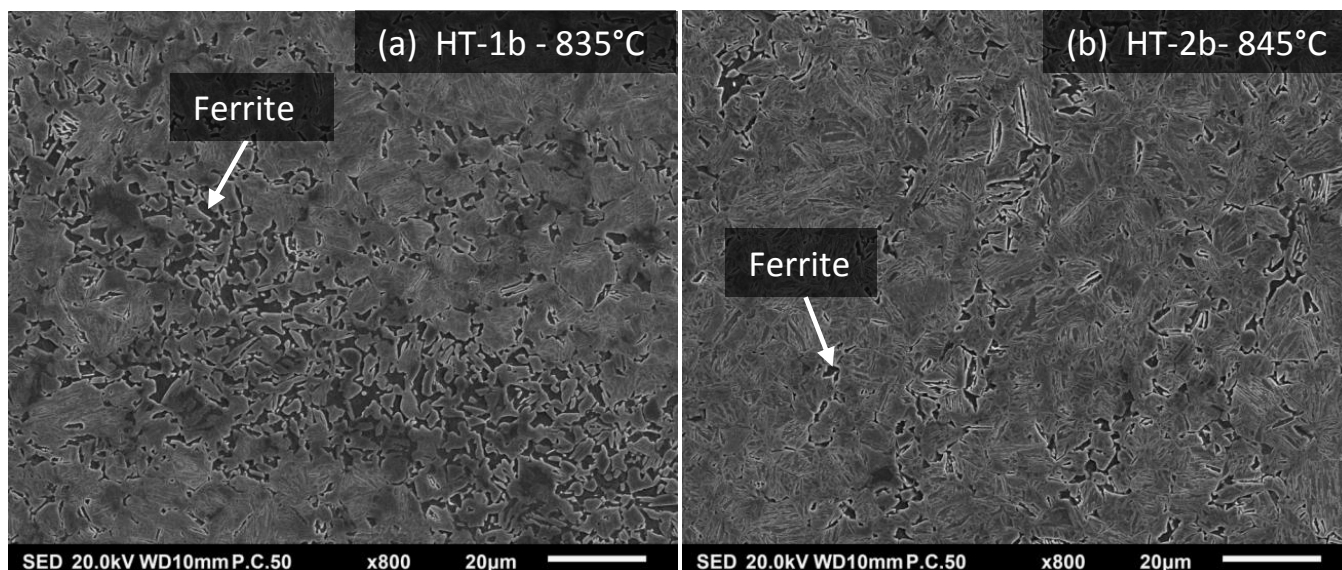


Figure 4.5: SEM images of heat treatments (a) HT-1b and (b) HT-2b with intercritical annealing temperatures of 835°C and 845°C, respectively. The microstructure consists of ferrite grains (dark) in a matrix of martensite and austenite.

to be overcome [11], omitting this step will result in an earlier observable phase transformation.

To determine the ferrite fraction at the start of the 400°C isothermal hold, samples from heat treatments HT-1b and HT-2b were studied using SEM. Figures 4.2b and 4.2c provide the ferrite fractions after cooling to 400°C obtained through image analysis (Section 3.6). A few examples of the resulting microstructures are given in Figure 4.5.

Heat treatment HT-3 made use of a cooling rate of 30°C/s to cool from intercritical temperatures to 400°C. This meant helium gas had to be used as coolant, which introduced an error (see Section 4.3). However, this cooling rate proved high enough to prevent any significant phase transformations during cooling. Therefore, the ferrite fraction from heat treatment HT-3a is considered to remain constant during cooling. In Figure 4.6 some of the microstructures from heat treatment HT-3a are shown, which show a considerable amount of ferrite.

4.2.3 Carbon Enrichment of Austenite

During heat treatments HT-1b, HT-2b and HT-3a, where the samples were quenched before bainite formation, a significant shift in M_s temperature was observed (as shown in Figure 4.7). From available literature [68–70] it is known that an increase in the carbon concentration of austenite will result in a shift of M_s towards lower temperatures. An increased carbon concentration will stabilise the austenite and lower temperatures (larger driving force for transformation) are needed

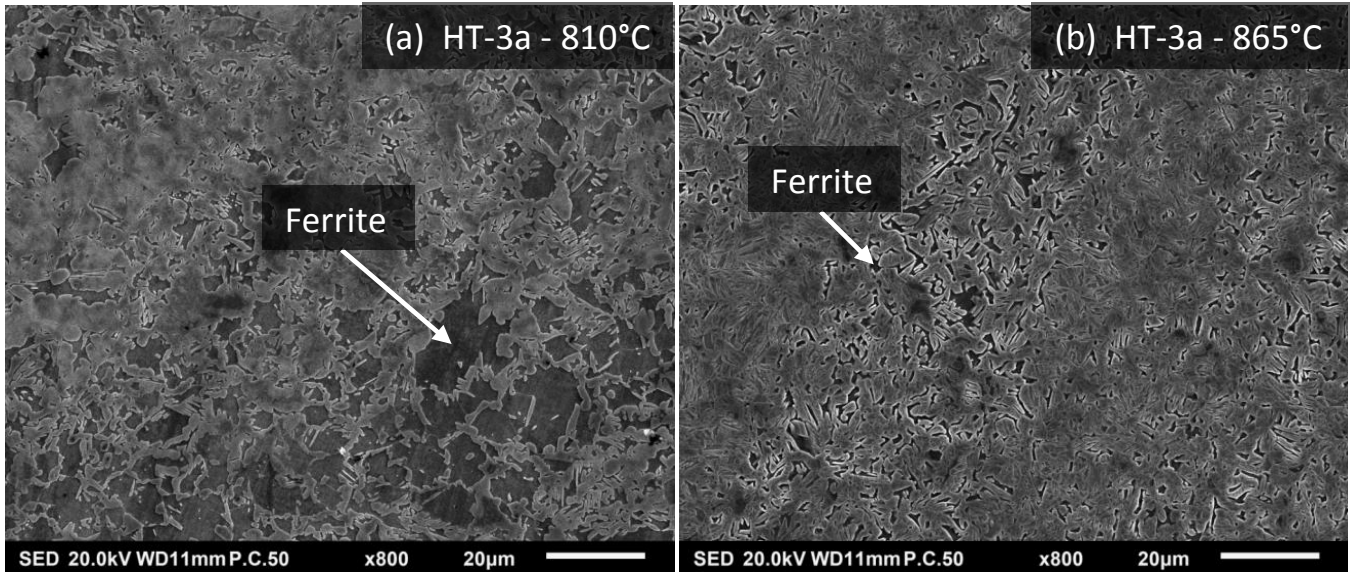


Figure 4.6: SEM images of heat treatments HT-3a with intercritical annealing temperatures of (a) 810°C and (b) 845°C. The microstructure consists of ferrite grains (dark) in a matrix of martensite and austenite.

to transform the austenite to martensite. Because there is very little room for carbon in the bcc structure, the austenite in this study becomes increasingly enriched in carbon with increasing ferrite fractions. This results in the observed shift in M_s . In the work of Mahieu et al. [71], Zhou et al. [72] and Dong et al. [73] an empirical equation was successfully used to estimate the M_s temperature using the chemical composition of the material:

$$M_s = 539 - 423C - 30.4Mn - 7.5Si + 30Al \quad (\text{in wt}\%) \quad (4.1)$$

Rewriting Equation 4.1, the carbon concentration in austenite can be estimated if all other concentrations are known:

$$C = \frac{(M_s - 539 + 30.4Mn + 7.5Si - 30Al)}{-423} \quad (\text{in wt}\%) \quad (4.2)$$

To approximate the carbon concentrations in austenite using Equation 4.2, a nominal composition of 3 wt% manganese and 2 wt% silicon was assumed. As these elements tend to segregate to austenite and ferrite, respectively, real values may slightly defer. However, as pointed out earlier, the diffusion of manganese and silicon is very sluggish and no large concentration differences are expected to form between ferrite and austenite, as annealing times are relatively short. Banding of the initial microstructure may also introduce a deviation from the nominal composition, but is not included in this approximation. The results of the calculations are shown in Figure 4.7 and it

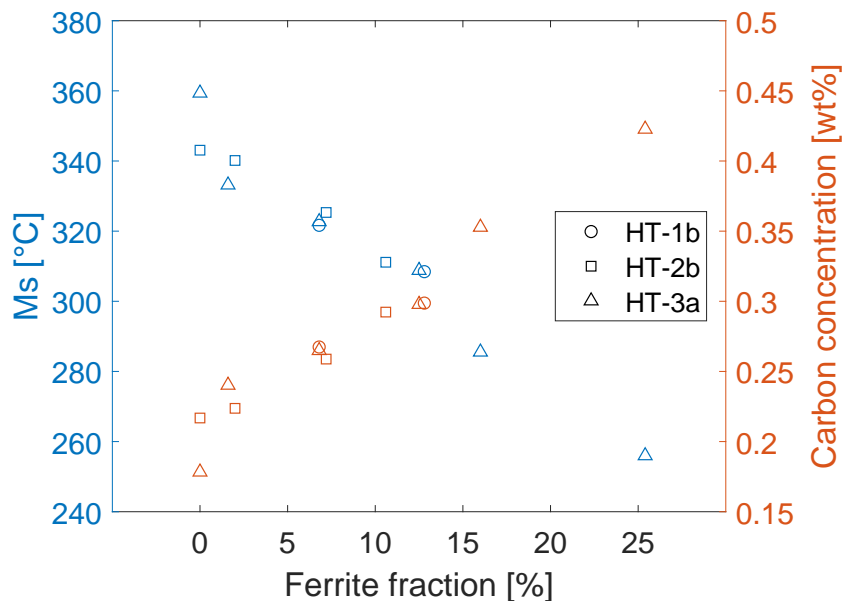


Figure 4.7: The shift in martensite start temperature (M_s) and the related carbon enrichment of austenite as a function of ferrite fraction in experiments HT-1b (circles), HT-2b (squares) and HT-3a (triangles).

can be seen that the carbon concentration in austenite is predicted to be nearly nominal when the sample has been fully austenitised. It can also be seen that the ferrite fraction and the shift in M_s (and thus the austenite carbon concentration) correlate well to each other, which indicates that the ferrite fractions were determined correctly.

In heat treatments HT-1b, HT-2b and HT-3a, where the material was quenched after ferrite had been formed/retained, the effect of carbon enrichment in austenite on the martensite transformation was observed. It is expected that a similar effect will occur for the bainite transformation and that the bainite start temperature, B_s , is also shifted to lower temperatures for increasing ferrite fractions. The carbon enrichment of austenite lowers the driving force for bainite formation and thus slows down the bainite transformation. As explained in Section 2.2.4 this may eventually result in the IRP (incomplete reaction phenomenon), where the formation of ferrite and bainitic ferrite have enriched the austenite in carbon to such a degree that no further transformation is feasible at the bainite formation temperature. The bainite transformation is incomplete and a significant fraction of austenite is left. This concept is also discussed in the works of Quidort and Brechet [4] and Zhu et al. [5] in relation to the effect of ferrite on bainite formation. From the results in Figure 4.7 it may be evident that increasing the ferrite fraction results in an increased carbon concentration of austenite and thus an increased stabilisation of austenite. Enlarging the ferrite fraction will therefore result in a local retardation of bainite formation, which may surpass any accelerating effects. In addition, the maximum fraction of bainite that can be formed before bainite formation ceases (IRP) is also decreased with increasing carbon concentrations in austenite and thus with

increasing ferrite fraction.

4.2.4 Ferrite Morphology

The material in this study was not homogenised and as a result the initial banded microstructure shown in Figure 3.1 influences the formation and retention of ferrite. As the initial microstructure showed ferrite grains that were ordered in bands, it is clear that the retained ferrite grains are also located in bands. The bands in this material are mainly caused by manganese segregation during solidification, leaving high-manganese and low-manganese areas. Manganese acts as an austenite stabiliser, with as consequence that ferrite prefers to be located in low-manganese areas. As manganese diffuses very slowly, this inhomogeneity is still present after the intercritical isothermal hold. Therefore, ferrite formed during cooling still prefers a banded microstructure.

Ferrite Formed During Cooling

In heat treatments HT-1 and HT-2 the ferrite fraction becomes very small during the intercritical isothermal hold (see Figures 4.2b and 4.2c). The ferrite fraction increases again during slow cooling due to the formation of new ferrite. This process is schematically shown in Figure 4.8 and the results can be observed when the ferrite morphology of heat treatments HT-1b and HT-2b is studied. As mentioned in Chapter 2, ferrite forms via nucleation and growth. Preferable nucleation sites include the austenite grain boundaries and ferrite that forms at these boundaries is called allotriomorphic ferrite. These allotriomorphs often grow along the austenite grain boundary, before growing into the austenite grain itself [11].

In Table 4.2 an overview is given of the different ferrite morphologies that are formed in heat treatments HT-1b and HT-2b. For low annealing temperatures (high ferrite fractions) the ferrite grains take on a variety of shapes. There are elongated allotriomorphs (E in Figure 4.9a) that have grown along the austenite grain boundaries. In addition, there are ferrite grains characterised as ‘irregular - type 1’ (i1 in Figure 4.9a), which often display one or more straight sections of grain boundary. It is believed that these grains have grown beyond the elongated allotriomorphic state and have started to grow into the austenite grain. In the middle of the low-manganese bands the i1 ferrite grains are very close to each other and have often merged to form a continuous ferrite section (C in Figure 4.9b). For intermediate annealing temperatures the ‘continuous’ ferrite grains are not observed and the i1 ferrite grains have become smaller in size and amount. Elongated allotriomorphs are still present for the intermediate annealing temperatures. An increase in elongated ferrite grains in a parallel arrangement (P in Figure 4.9a) is also noticed. These ferrite grains are believed to have a bainitic or Widmanstätten ferrite origin and sometimes also appear in a more feathery structure. For high annealing temperatures only two types of ferrite grains are observed.

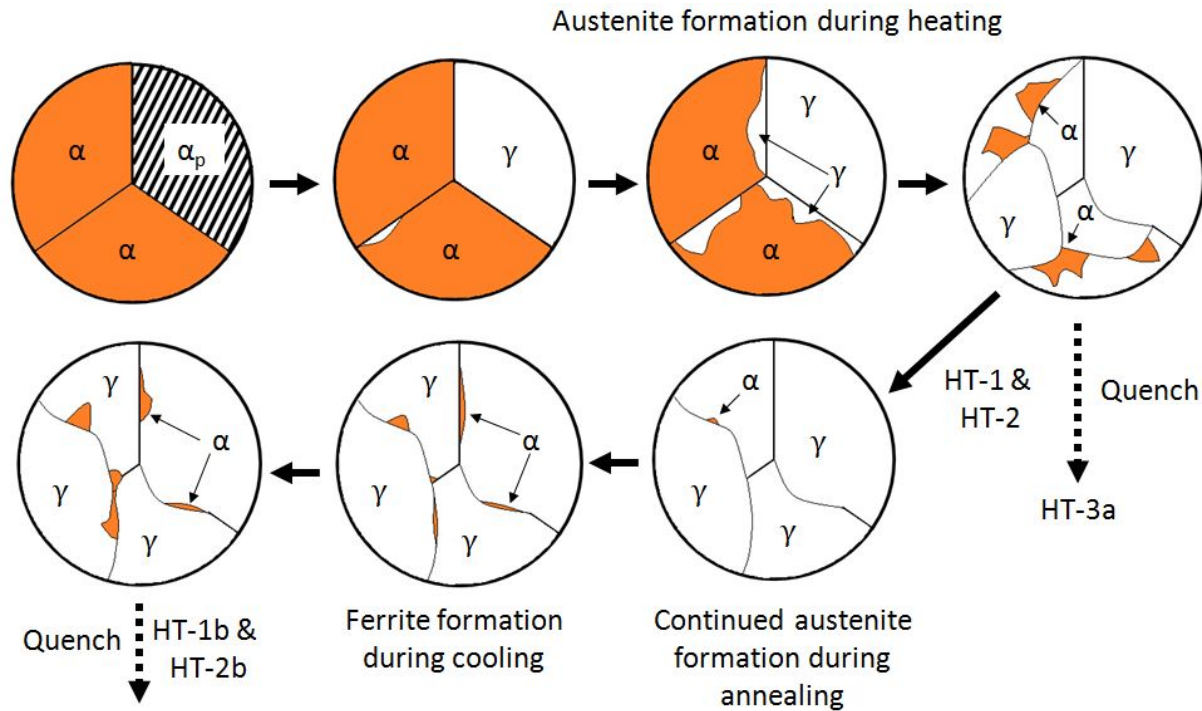


Figure 4.8: Schematic representation of the evolution of ferrite and austenite during intercritical annealing and subsequent slow cooling. The formation of martensite during the final quench is not represented in this figure.

The elongated allotriomorphs are still present, but there is also the rise of a new morphological feature, which is characterised as ‘tree-like’ (T in Figure 4.9c). These ‘tree-like’ ferrite grains have a highly irregular branch-like structure and possibly form the stage between elongated allotriomorphs and the il ferrite grains, or are an early stage of bainite formation.

The effect of heating rate can also be observed. The evolution of ferrite morphology with annealing temperature seems to be faster for heat treatment HT-2b than for heat treatment HT-1b. Looking at Figures 4.2b and 4.2c, this coincides with the degree in which the ferrite fraction decreases in both heat treatments. It follows that the ferrite fraction that is obtained is a measure for the degree to which ferrite was allowed to develop and thus is a determining factor in the final ferrite morphology.

Ferrite Retained Through Intercritical Annealing

In heat treatment HT-3 ferrite was retained through intercritical annealing. It was austenite that grew, rather than ferrite, which resulted in rounded austenite grain boundaries. A consequence is that the ferrite grains obtained a sharp and jagged appearance. By studying the samples of heat treatment HT-3a the morphological evolution of ferrite in this heat treatment could be followed and is summarised in Table 4.3. With increasing annealing temperatures the ferrite grains progress from the initial polygonal grains, via a ‘blocky’ morphology (b in Figure 4.10a), to smaller ‘irregular -

Table 4.2: Ferrite morphology as a function of annealing temperature in heat treatments HT-1b and HT-2b. Presence is indicated by a check-mark and absence by a cross. If a morphology is present, but not in abundance, this is indicated with a dotted circle.

		Annealing temperature					
		HT-1b		HT-2b			
Morphological Feature	Abbreviation	835°C	875°C	845°C	855°C	865°C	950°C
Elongated allotriomorph	E	✓	✓	✓	✓	✓	✗
Irregular - type 1	i1	✓	✓	✓	✓	⊙	✗
Continuous	C	✓	✗	✓	✗	✗	✗
Parallel	P	⊙	✓	✓	✓	✗	✗
Tree-like	T	✗	⊙	✗	⊙	✓	✗

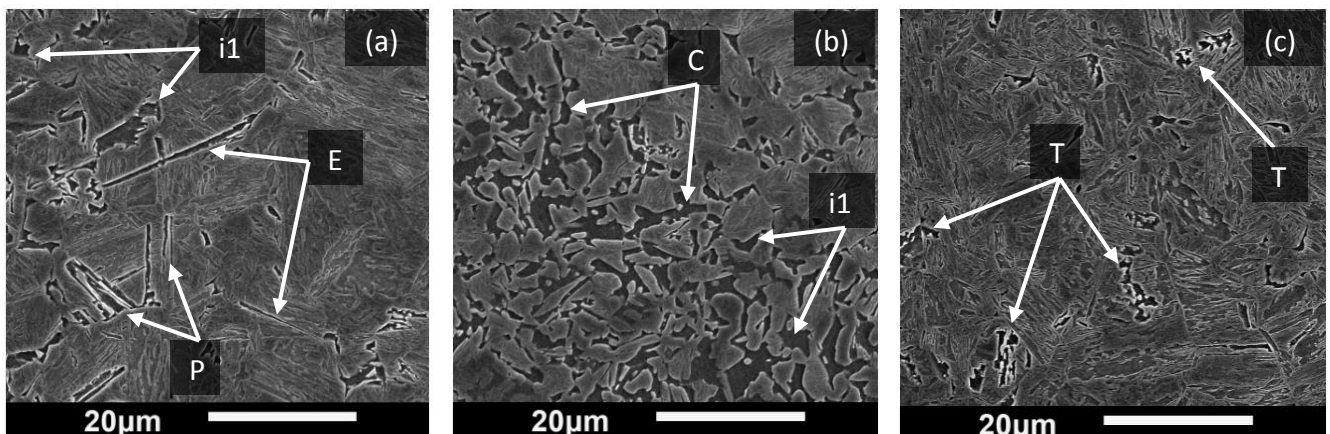


Figure 4.9: Examples of ferrite morphologies found in samples from heat treatments HT-1c and HT-2c.

Table 4.3: Ferrite morphology as a function of annealing temperature in heat treatment HT-3a. Presence is indicated by a check-mark and absence by a cross. If a morphology is present, but not in abundance, this is indicated with a dotted circle.

		Annealing temperature					
		HT-3a					
Morphological Feature	Abbreviation	810°C	850°C	865°C	880°C	900°C	950°C
Blocky ferrite	b	✓	⊙	✗	✗	✗	✗
Irregular - type 2	i2	✓	✓	✓	✓	✓	✗
Bainitic remains	B	✓	⊙	✓	⊙	✗	✗

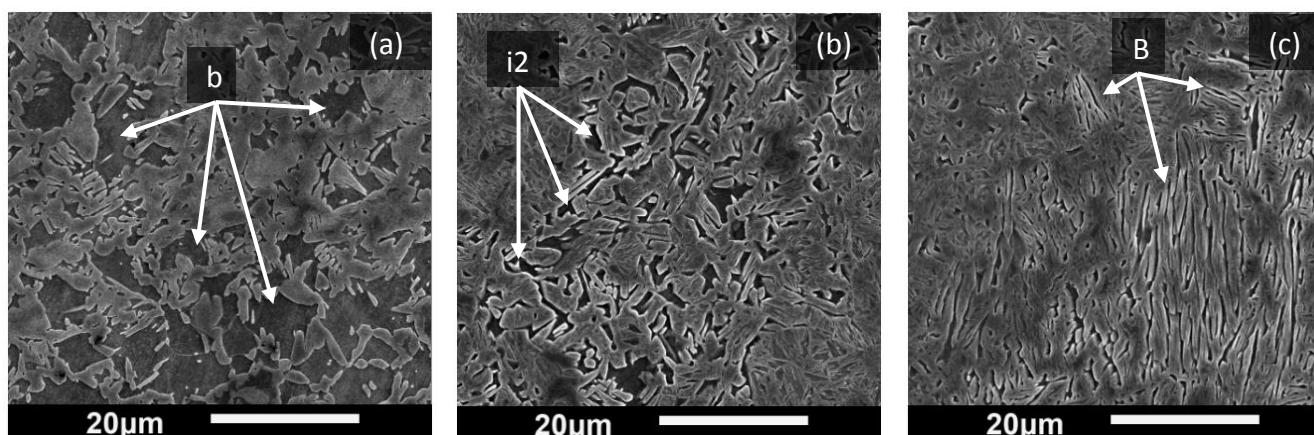


Figure 4.10: Examples of ferrite morphologies found in samples from heat treatment HT-3a.

type 2' ferrite grains (i2 in Figure 4.10b). This process is also schematically shown in Figure 4.8. In addition to ferrite, the bainitic ferrite structures found in the initial microstructure (Figure 3.1) are also partly retained. These bainite structures are arranged in packets, where the bainite sheaves have a similar (parallel) orientation (B in Figure 4.10c). Within these packets, austenite has grown and therefore the bainite sheaves have become narrower. Ferrite grains and 'bainitic remains' become smaller in both size and amount with increasing annealing temperatures.

Prior Austenite Grain Size

The prior austenite grain size (PAGS) is a microstructural feature that influences the total interfacial area and thus the bainite formation kinetics. In the works of Lee et al. [74] and Lan et al. [75] it was found that a smaller PAGS can lead to an acceleration of the bainite formation kinetics. It

is argued [74, 75] that a smaller PAGES increases the amount of austenite/austenite interfacial area in a material and thus increases the amount of bainite nucleation sites. However, in the works of Xu et al. [76] and Hu et al. [77] it is found that smaller PAGES's impede the bainite sheaf growth. They [76, 77] consider that during bainite formation, the growth rate of bainite sheaves is more important than the initial nucleation, when the rate of bainite formation is considered. From this viewpoint, larger PAGES's will result in an acceleration of bainite formation kinetics, as they will allow more volume for bainite sheaves to grow unrestricted.

To include the effect of PAGES in this study, the martensitic structures in the quenched samples from heat treatments HT-1b, HT-2b and HT-3a, with top temperatures of 875°C, 865°C and 880°C, respectively, were studied using SEM imaging. It was found that the PAGES for the samples from HT-1b and HT-2b were within the range of 10-20 μm (further referred to as 'large'). The PAGES resulting from heat treatment HT-3a were smaller, with an approximate range of 5-15 μm (further referred to as 'small'). This smaller grain size could be explained by the fact that the material spends less time at high temperatures in heat treatment HT-3 than in heat treatments HT-1 and HT-2, providing less time for austenite to grow and develop. Although the difference in PAGES's is not large, it may still have an effect on the subsequent bainite formation kinetics.

4.2.5 Segregation of Alloying Elements

An additional angle with respect to ferrite formation through intercritical annealing is found in the segregation of alloying elements at the ferrite/austenite interface. In several previous studies [78–82] peaks in alloying element concentrations were found at ferrite/austenite interfaces during intercritical annealing. These peaks were observed when new ferrite was formed [78, 79] as well as when ferrite was retained [80–82]. The peaks are caused by the solubility of the alloying elements in ferrite and austenite, respectively. At the ferrite/austenite interface these elements tend to segregate to the phase that can accommodate the highest concentration of these elements, in order to establish thermodynamic equilibrium between both phases. An increased concentration of manganese and/or carbon or a decreased concentration of silicon in the austenite near the ferrite/austenite interfaces could make it more difficult for any bainite to form, as it will increase the chemical stability of the austenite in this region. Therefore, elemental segregation might result in a decrease (or increase for opposite conditions) of the bainite formation rate.

Thermo-Calc DICTRA software with TCFE9 and MOBFE4 databases was used to validate the observations in the literature for the material and heat treatments in this study. For these simulations two heat treatments were used, as given in Figures 4.12a and 4.12b. From these figures it can be seen that heat treatments A and B resemble heat treatments HT-1 and HT-3, respectively,

and thus vary in heating rate, cooling rate and the presence of an intercritical isothermal hold. Intercritical temperatures were both set at 810°C for comparison. Paraequilibrium starting conditions were assumed, where carbon was in full equilibrium, but manganese and silicon were set for both phases at nominal values of 3 wt% and 2 wt%, respectively. An overview of the simulation starting conditions is given in Figure 4.11. It was assumed that the first stage of austenite formation had just finished and only austenite and ferrite were left. The effects of banding were not considered.

The simulation results are shown in Figures 4.13a and 4.13b. The progression of austenite formation during the intercritical isothermal hold in heat treatments HT-1 and HT-2 was confirmed by the simulations and cause the shift of the manganese peak in Figure 4.13a. For all heat treatments a large spike in manganese is seen at the ferrite/austenite interface during cooling. Furthermore, due to the high cooling rate used in heat treatment B, this heat treatment also shows a carbon peak, meaning that the cooling rate does not allow full redistribution of carbon. In heat treatment B, a local depletion in silicon can also be found (Figure 4.13b). Besides ferrite formation during cooling in heat treatment A, the simulation also predicted some ferrite formation ($\approx 1\%$) during cooling in heat treatment B. Both the simulated elemental segregations are thought to have a decelerating effect on bainite formation. This effect is larger for heat treatment B due to the larger manganese and carbon peaks, which locally increase austenite stability.

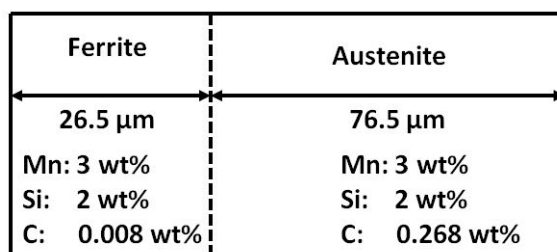


Figure 4.11: Simulation cell used in the Thermo-Calc DICTRA simulations.

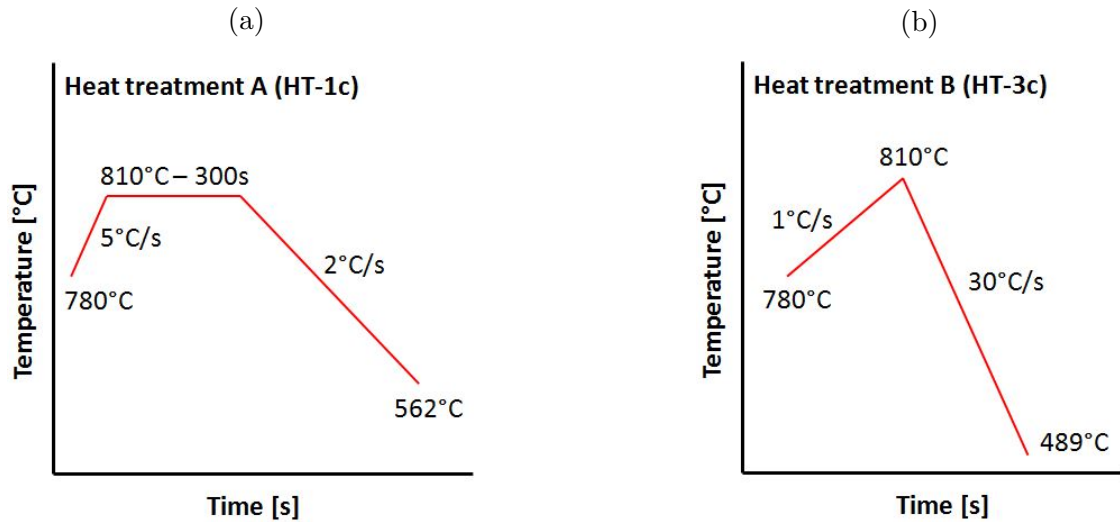


Figure 4.12: Heat treatments used for the Thermo-Calc DICTRA simulations.

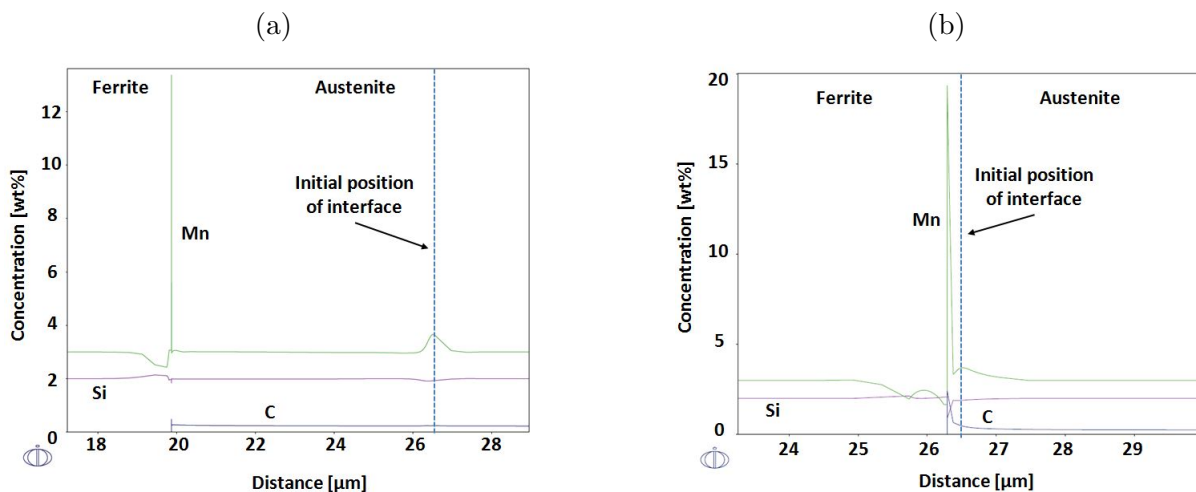


Figure 4.13: Thermo-Calc DICTRA simulations of (a) heat treatment A and (b) heat treatment B showing the segregation of alloying elements Mn, Si and C at the ferrite/austenite interface.

4.2.6 Prior Ferrite Summary

In Section 4.2 it was shown that during heat treatments HT-1 and HT-2 austenite continued to grow during the intercritical isothermal hold and ferrite was formed during cooling to 400°C. Contrarily, in heat treatment HT-3 ferrite was retained from the initial microstructure and no significant additional ferrite formation was observed during cooling. The difference between ferrite formation and ferrite retention resulted in a difference in ferrite morphology. The grown ferrite displayed more rounded grains and also contained allotriomorphs. The retained ferrite had a jagged appearance and included large blocky ferrite grains at the higher ferrite fractions. Ferrite formation was also shown to have an effect on the carbon concentration in austenite, where the austenite gets increasingly enriched with carbon with increasing ferrite fraction. In addition, literature and simulations have shown the

Table 4.4: Summary of the findings related to ferrite formation/retention. Explanations of abbreviations can be found in the nomenclature.

HT	HR [°C/s]	TT [°C]	CR [°C/s]	f_{α} [%]	C_{γ} [wt%]	α - morph	PAGS	C- spike	Mn- spike	Si- drop
HT-1c	5	835	2	13	0.30	E,i1,P,C	Large	Negl.	Narrow	Negl.
HT-1c	5	875	2	7	0.27	E,i1,P,T	Large	Negl.	Narrow	Negl.
HT-2c	10	845	2	11	0.29	E,i1,P,C	Large	?	?	?
HT-2c	10	855	2	7	0.26	E,i1,P,T	Large	?	?	?
HT-2c	10	865	2	2	0.22	E,i1,T	Large	?	?	?
HT-2c	10	950	2	0	0.22	-	Large	-	-	-
HT-3c	1	810	30	25	0.42	i2,B,b	Small	Yes	Broad	Yes
HT-3c	1	850	30	16	0.35	i2,B,b	Small	Yes	Broad	Yes
HT-3c	1	865	30	13	0.30	i2,B	Small	Yes	Broad	Yes
HT-3c	1	880	30	7	0.26	i2,B	Small	Yes	Broad	Yes
HT-3c	1	900	30	2	0.24	i2	Small	Yes	Broad	Yes
HT-3c	1	950	30	0	0.18	-	Small	-	-	-

presence of elemental concentration spikes at the ferrite/austenite interfaces as a result of elemental segregation during intercritical annealing and subsequent cooling. The findings of Section 4.2 have been summarised in Table 4.4.

4.3 Bainite Formation

In heat treatments HT-1c, HT-2c and HT-3c the intercritically annealed material is cooled to 400°C. It is isothermally held at this temperature for 1500 (HT-1c and HT-2c) or 1800 (HT-3c) seconds during which bainite is formed. As described in Section 3.2, the formation of bainitic ferrite can be seen in the dilatometry data as an expansion of the sample.

4.3.1 Bainite Formation

Figure 4.14a shows the sample expansion recorded by the dilatometer during bainite formation in heat treatments HT-1c (dotted lines) and HT-2c (continuous lines). In Figure 4.14b the corresponding derivatives with respect to time are shown, which indicate the rate at which the formation of bainite progresses. A higher rate of bainite formation is characterised by a larger inclination of the curve in Figure 4.14a and a higher peak in Figure 4.14b. From these figures it can be seen that bainite starts to form quickly in the presence of ferrite, whereas without ferrite, the formation of bainite starts slowly. By looking at the maxima of the derivatives shown in Figure 4.14b it can also

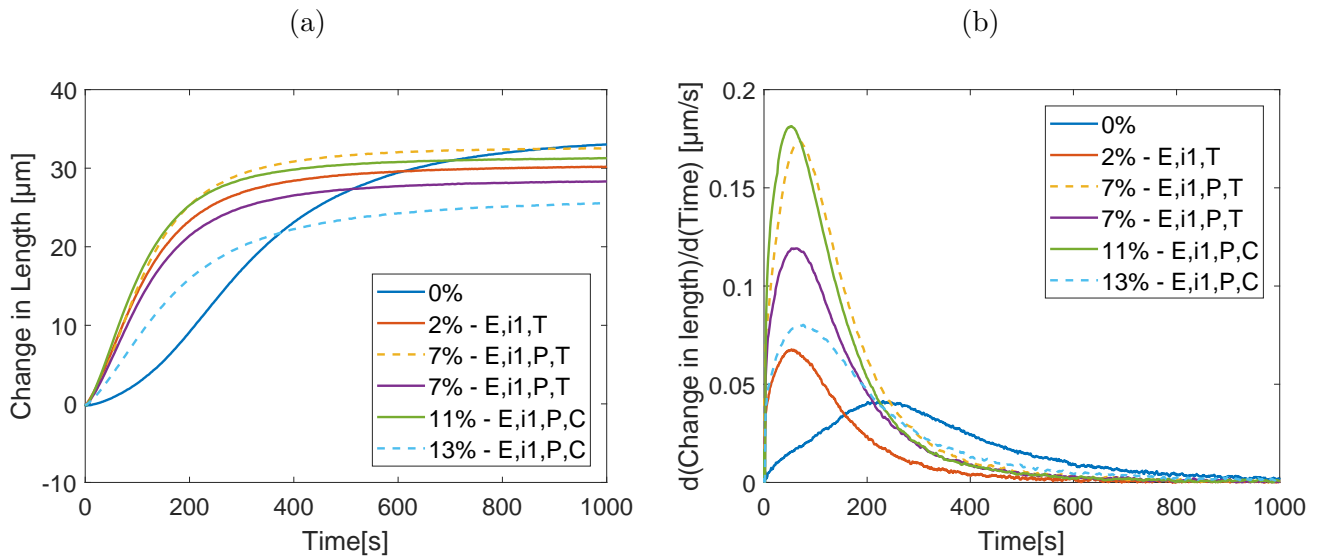


Figure 4.14: Expansion data (a) and their derivatives (b) of the first 1000 seconds of bainite formation in heat treatments HT-1c (dotted lines, heating rate of 5°C/s) and HT-2c (continuous lines, heating rate of 10°C/s). The legend indicates both ferrite fractions and ferrite morphologies.

be seen that the bainite formation rates in the presence of ferrite are high when compared to the fully austenitised condition.

In Figure 4.15a the expansion during bainite formation in heat treatment HT-3c is shown, with the corresponding derivatives (with respect to time) in Figure 4.15b. It can be seen that during the first 15 seconds of bainite formation the curves experience a jump in data, which can be seen more clearly in the magnified image of Figure 4.16. It is believed that the jump in expansion data at 9 to 10 seconds is caused by a measurement error. Furthermore, it is possible (something which is also proposed in the work by Ravi et al. [3]) that there is a systematic error of 1 μm to 2 μm that is located on top of the bainite expansion data. Several experiments were carried out to investigate the cause and size of the total error, but no definitive conclusion could be made. The error experiments and further remarks on this topic can be found in Appendix B. For this study, the first 20 seconds of this heat treatment will not be used to base any direct conclusions on. The error displays repetitive behaviour and therefore the data after the first 20 seconds can still be used, as each of the curves experienced the error.

In Figure 4.15b it can be seen that the presence of 2% ferrite significantly accelerates the formation of bainite. This accelerating effect decreases with increasing ferrite fraction. Due to the measurement error it can not be said with certainty if all ferrite fractions result in higher (maximum) bainite formation rates when compared to the case of 0% ferrite. However, what can be concluded is that

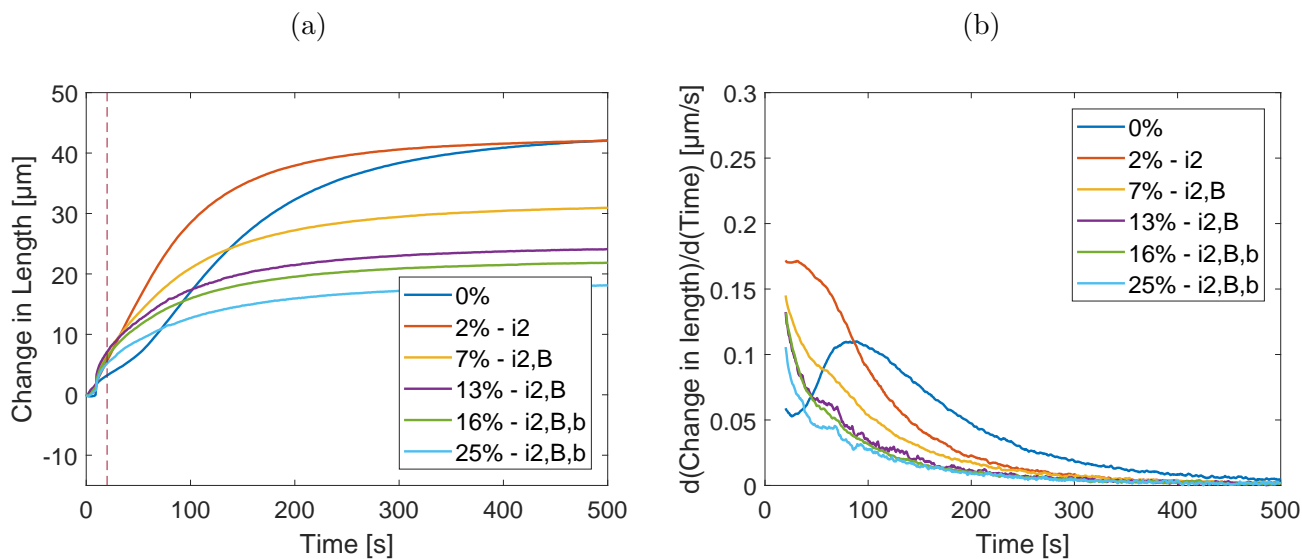


Figure 4.15: Expansion data (a) and their derivatives (b) of the first 500 seconds of bainite formation in heat treatment HT-3c. The data left of the vertical dotted line is heavily affected by the measurement error (see Appendix B) and is therefore omitted in (b). The legend indicates both ferrite fractions and ferrite morphologies.

the formation of bainite in the presence of ferrite occurs in a significantly smaller time span when compared to bainite formation in the absence of ferrite.

4.3.2 Bainite Formation Kinetics

Interfacial Area

For all bainite heat treatments a quick start of bainite formation is observed in the presence of ferrite. This can be explained by considering the available nucleation sites for bainite formation. These nucleation sites consist of high energy locations like austenite/austenite interfaces, as explained in Section 4.2. By the formation of ferrite additional interfacial area is created, as ferrite/austenite interfaces are formed. This results in an increase in the total number of preferential nucleation sites. Therefore, bainite is able to nucleate (and subsequently grow) in an increased amount of locations, resulting in an increased initial bainite formation rate. When no ferrite is present, the amount of preferential nucleation sites is not increased, resulting in a slower start of bainite formation.

Autocatalytic Nucleation

From Figures 4.14b and 4.15b it can be seen that the maxima of the derivatives are higher in the presence of ferrite than in the absence of ferrite. As these derivatives indicate the bainite formation rate, it follows that the maximum bainite formation rate that is achieved is higher in the presence of

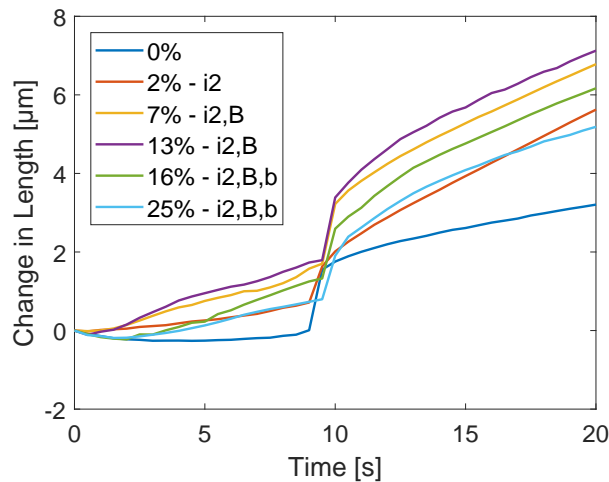


Figure 4.16: Magnification of the measurement errors experienced at around 10 seconds after the start of the 400°C isothermal hold.

ferrite. These high maximum growth rates are believed to be the result of an increase in the amount of bainite sheaves that start to form simultaneously when ferrite is present. As discussed before, the presence of ferrite results in an increased amount of locations where bainite can nucleate and grow from. After the first bainite sub-unit has formed, a bainite sheaf grows through autocatalytic nucleation of new sub-units at the boundary of the previous sub-unit (as discussed in Chapter 2). If the presence of ferrite results in an increased amount of initial bainite sub-units, the amount of autocatalytic nucleation events is also increased. Therefore, more bainite sub-units start to nucleate and grow simultaneously, resulting in the higher (maximum) bainite transformation rate that is observed in the presence of ferrite.

Carbon Enrichment

In Section 4.2.3 it was discussed that the carbon concentration in austenite increases with increasing ferrite fraction, resulting in increased austenite stability and less driving force for the formation of bainite. This has two consequences. First of all, the fraction of bainite that can be formed before the T'_0 limit is reached becomes smaller when the ferrite fraction increases. Therefore, for larger ferrite fractions, a smaller amount of bainite can be formed before the bainite transformation comes to a halt (IRP). A second consequence is that the increased stability of austenite slows down the bainite formation kinetics. This explains the decrease in bainite formation rates with increasing ferrite fractions in heat treatments HT-1c and HT-3c, indicated by the derivatives in Figures 4.14b and 4.15b, respectively. In these figures it can be seen that when the ferrite fraction is increased, the maximum bainite formation rate (maximum of the derivative) becomes smaller. The increased austenite stability also influences the decline of the bainite formation rate after a maximum has been reached, as the formation of bainitic ferrite further increases the carbon concentration in austenite.

Naturally, this decline is also affected by the amount of remaining austenite during bainite formation as there will be a decreasing amount of space where bainite may form.

For heat treatment HT-2c, the effect of ferrite on bainite formation kinetics seems to have shifted, as larger ferrite fractions are needed to produce behaviour similar to that observed in HT-1c for lower ferrite fractions. As can be seen from Tables 4.9 and 4.10 the carbon concentration in austenite, ferrite morphology and PAGS (all with respect to ferrite fraction) are very similar for heat treatments HT-1c and HT-2c. This suggests that the shift in effect of ferrite fraction on bainite formation kinetics has its origin in the difference in heating rate and/or annealing temperature, which may affect the elemental distribution within the material. However, with the current data no explanation could be found for the difference in bainite formation kinetics with respect to ferrite fraction and this topic is therefore recommended for future research.

Prior Austenite Grain Size

In Figures 4.14a and 4.15a the bainite formation curves were shown. However, for comparison between the individual treatments these figures are not very clear. Therefore, individual curves, having the same ferrite fraction and comparable carbon concentrations in austenite (Table 4.4), are shown together in Figures 4.17a to 4.17d. As mentioned in Section 4.2.4 bainite formation reaches a limit where austenite is enriched in carbon to a point where no further bainite formation is possible. For all of the experiments in this study this limit is reached during the 400°C isothermal hold. Considering that the carbon concentration in austenite is a function of the total amount of bcc phase (ferrite and bainitic ferrite), it may be deduced that the total amount of bainite formed is the same for each experiment that started with the same ferrite fraction. In Figures 4.17a to 4.17d each of the curves is therefore normalised by dividing the change in length by the maximum achieved change in length (as a result of bainite formation). This makes it possible to compare curves with the same ferrite fraction without the interference of factors that may have influenced the lattice parameter (and thus length measurement) during the dilatometry measurements (such as local carbon distribution [67]).

In each of the Figures 4.17a to 4.17d it can be seen that the formation of bainite is faster in heat treatment HT-3c than in heat treatments HT-1c and HT-2c. This results in a shorter overall bainite formation time (the time until the maximum bainite fraction is reached). This can also be deduced by comparing Figure 4.14b and Figure 4.15b, where it is shown that the bainite formation rate returns to zero faster in heat treatment HT-3c than in heat treatments HT-1c and HT-2c. The fact that this effect is also noticed in the fully austenitised samples (Figure 4.17a) indicates that it is not (fully) dependent on the formation of ferrite. A logical step would be to consider the PAGS. As mentioned before in Section 4.2.4, the effect of PAGS on the bainite formation kinetics is still

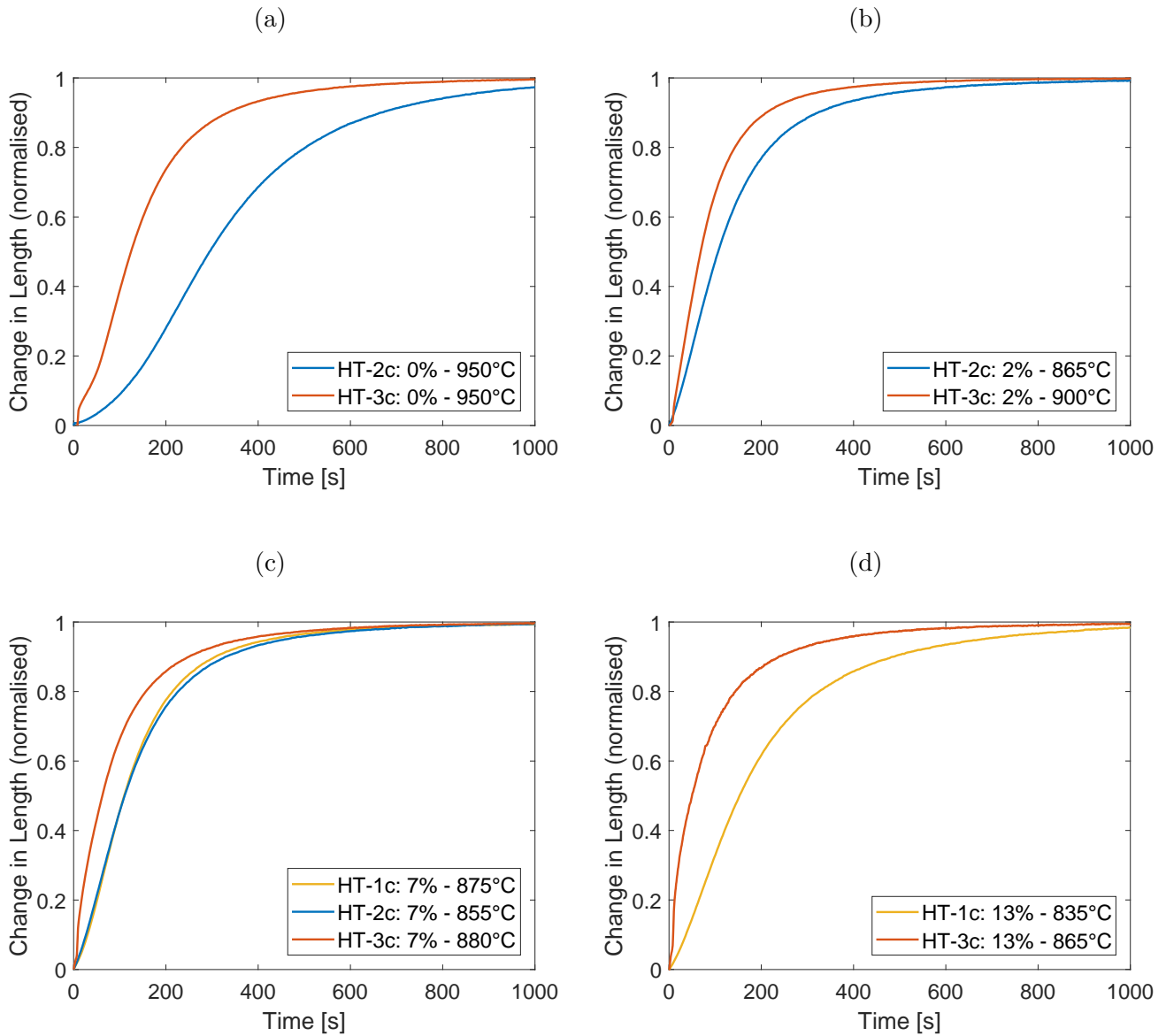


Figure 4.17: Comparison of sample expansion during bainite formation between heat treatments with (a) 0% ferrite, (b) 2% ferrite, (c) 7% ferrite and (d) 13% ferrite. Each curve is normalised by dividing the sample expansion during bainite formation by the total amount of expansion due to formation of bainite. Note: the error in the HT-3c curves has not been modified and is still present.

unclear, with both smaller [74, 75] and larger [76, 77] PAGES's being suggested to increase bainite formation kinetics. Samples in HT-3c, having a smaller PAGES, show an increased bainite formation rate when compared to samples with a larger PAGES (HT-1c and HT2c). This indicates that in this case a smaller PAGES is preferential for accelerating the bainite formation kinetics.

Ferrite Morphology

From Tables 4.9 and 4.10 it can be seen that there are considerable changes in ferrite morphology, depending on heat treatment temperature and the manner in which ferrite was obtained. Parameters like ferrite fraction, PAGES and carbon concentration in austenite interfere with a detailed analysis of the effects of different ferrite morphologies on the bainite formation kinetics. However, possible effects may be theorised.

From Figure 4.17a it can be seen that there is a large kinetic difference between the 0% ferrite bainite formation curve obtained from heat treatment HT-2c and the 0% ferrite bainite formation curve obtained from heat treatment HT-3c. As mentioned before, this difference is thought to be due to the effect of PAGES. From Figures 4.17b and 4.17c it can be seen that the kinetic difference between heat treatments that produce the same ferrite fractions becomes significantly smaller. Although annealing temperatures are not equal anymore (which would affect the PAGES), this could indicate that the E, T and possibly i1 morphologies are more efficient than the i2 morphology in accelerating the bainite formation kinetics. The E and T morphologies offer a large interfacial area per ferrite fraction when compared to the more bulky i2 morphology. This results in an increased amount of possible bainite nucleation sites with respect to the volume of the ferrite grain. The i1 and i2 morphologies look similar, although the ferrite grain boundaries of the i2 morphology are much sharper. This could have an influence on bainite nucleation kinetics as well, but would require a more detailed study.

In Figure 4.17d it can be seen that the kinetic difference between the expansion curves enlarges again with the addition of the C morphology, which offers less interfacial area per ferrite grain volume than the E, T and i1 morphologies. There is also the increased presence of the B morphology, which offers a large interfacial area per ferrite grain volume. However, between the elongated ferrite grains in the B morphology, the space required for bainite growth (after nucleation) is very limited, which decreases the effectiveness of this morphology.

When the effect of ferrite morphology on bainite formation kinetics is considered, it has to be noted that the effects reported in this study are observed in a material that shows considerable banding. This results in ferrite grains that are locally closely packed and that are often of relatively large size. This decreases the overall efficiency of a certain ferrite fraction, as the increase in bainite

nucleation sites is localised and subsequent bainite sheaf growth can be hindered by neighbouring ferrite grains. In addition, large ferrite grains generally offer a smaller interfacial area per ferrite grain volume, and thus per ferrite fraction.

From the reasoning above, it can be deduced that for the acceleration of bainite formation kinetics it is preferential to have ferrite grains that are evenly dispersed throughout the material and offer a large interfacial area in comparison to their volume. The latter could be achieved by small ferrite grain sizes or elongated (narrow) ferrite grains.

Segregation of Alloying Elements

In Section 4.2.5 it was mentioned that concentration spikes of the alloying elements may exist at the ferrite/austenite interfaces. This would have a decelerating effect on subsequent bainite nucleation on these interfaces, something that is also found in the work of Zhu et al. [5]. With the aid of simplified Thermo-Calc DICTRA simulations it was shown that these concentration spikes can indeed be expected to be present and are slightly larger in heat treatment HT-3c than in heat treatments HT-1c and HT-2c. However, the expansion curves obtained with dilatometry (Figures 4.14a and 4.15a) clearly show an acceleration of bainite formation in the presence of ferrite, which is higher for the samples in heat treatment HT-3c. It is therefore suspected that the elemental concentration spikes in this study were not large enough to play a major role in the nucleation of bainite. Factors such as the increased amount of bainite nucleation sites (gained by the presence of ferrite) and carbon concentration in austenite seem to have a much stronger effect on the overall bainite formation kinetics in this study.

4.3.3 Bainite Morphology

Bainite can be characterised by a distinction between five different morphologies: granular bainite (GB), upper bainite (UB), degenerated upper bainite (DUB), lower bainite (LB) and degenerated lower bainite (DLB) [83]. Granular bainite consists of irregular grains of bainitic ferrite. The differences between upper bainite and lower bainite were discussed in Chapter 2. The term ‘degenerated’ refers to the presence of incomplete reaction products, such as retained austenite or martensite [83].

The morphology of bainite obtained during the different heat treatments was studied with the aid of SEM. In general, the bainite morphology obtained after heat treatments HT-1c, HT-2c and HT-3c can be described as a mixture of granular bainite and carbide free bainite (CFB). The latter is considered a type of DUB [84], where the bainite laths are surrounded by film-like austenite. In addition, blocky martensite-austenite (MA) constituents were observed, which consist of a mixture of retained austenite and martensite (formed during quenching to room temperature). However,

with increasing ferrite fraction a change in morphology was observed.

- When no ferrite was present (Figures 4.18a and 4.18b), the morphology consists of packets of lath-like CFB, where the bainite laths are arranged in similar orientations. The MA constituent is arranged in blocky islands which are relatively large when compared to those in the presence of (prior) ferrite.
- For low ferrite fractions (2%), the bainite morphology is similar to the morphology when no ferrite is present. However, the MA islands are smaller.
- When intermediate fractions of ferrite were present (7% - 13%, Figures 4.18c and 4.18d) the bainite morphology starts to change significantly. The lath-like CFB packets, observed when no ferrite was present, seem to get exchanged for more irregular structures. These structures can best be described as a (bainitic) ferrite matrix with islands of retained austenite or MA that are irregularly shaped with rounded edges. However, for heat treatment HT-3c also areas with large packets of parallel lath-like bainite are observed (such a packet is not visible in Figure 4.18d, but can be seen in Figure 4.18f). MA islands are present, but have significantly decreased in size when they are compared to the 0% ferrite morphology. Although ferrite grains were shown to prefer a banded microstructure (see Section 4.2.4), no effect of banding on the morphology of bainite could be distinguished in the presence of intermediate ferrite fractions.
- For large ferrite fractions (16% - 25%, Figures 4.18e and 4.18f) bainite consists almost entirely of GB. The areas with large packets described for intermediate ferrite fractions in heat treatment HT-3c are also observed for large ferrite fractions and are in contrast to the irregular GB structure. The MA islands have become smaller compared to intermediate ferrite fractions. Large ferrite grains in banded structures can also be distinguished.

The change in bainite morphology can be explained by the carbon enrichment of austenite with ferrite formation, as discussed in Section 4.2.3. In the work of Spanos et al. [85] it is shown that the carbon concentration in steels with 2% Mn affects the bainite morphology. Spanos et al. [85] show that when the carbon concentration of the steel is altered, a different bainite morphology can become dominant. With increasing prior ferrite fractions the remaining austenite is increasingly enriched with carbon which can be seen as a change of steel composition with respect to carbon. Therefore, it is suggested that the GB observed in this study is dominant at higher austenite carbon concentrations ($\gg 0.2\%$) and that the bainite morphology changes from predominantly DUB to predominantly GB as a result of carbon enrichment in austenite through the formation of ferrite.

It was observed that for intermediate to high ferrite fractions areas with large lath-like bainite packets are present in heat treatment HT-3c, but not in heat treatment HT-1c or HT-2c. It is believed that these packets are the result of the initial microstructure, which also contained areas with coarse bainite (see Figure 3.1). When higher ferrite fractions were retained during intercritical annealing, part of the ferrite in these bainitic areas was also retained, as was discussed in Section 4.2.4. In heat treatments HT-1c and HT-2c most of the ferrite formed during cooling and did not form any packets of lath-like ferrite structures. Therefore, these packets are not observed in the final bainitic microstructure of these heat treatments.

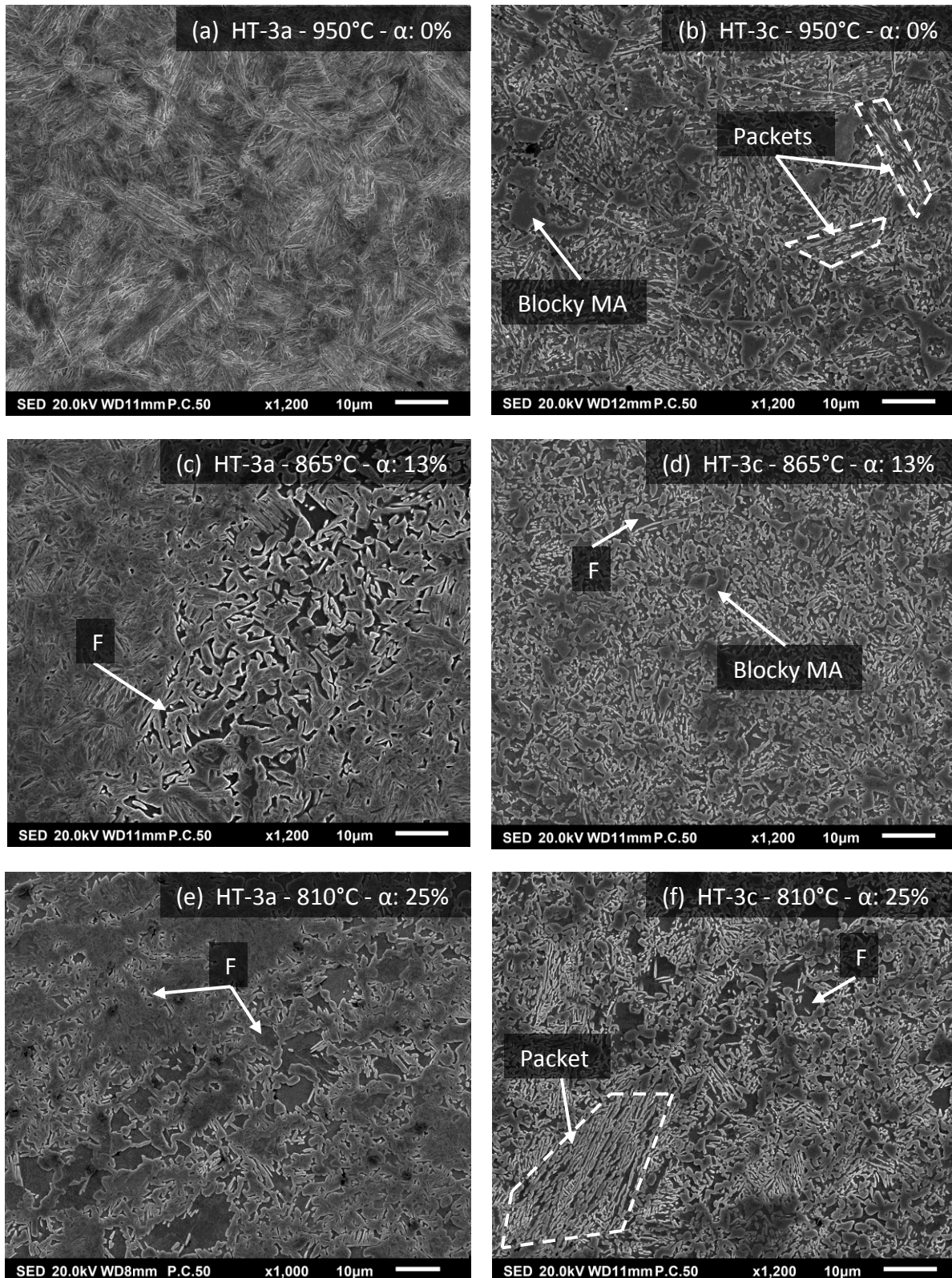


Figure 4.18: SEM images (a),(c) and (e) show the prior ferrite fractions and SEM images (b), (d) and (f) show the final bainite structures of heat treatment HT-3c with top temperatures of 950°C, 865°C and 810°C, respectively. F and MA denote the ferrite and martensite-austenite constituent, respectively. The evolution of bainite morphology with increasing ferrite fractions looks similar for heat treatments HT-1c and HT-2c.

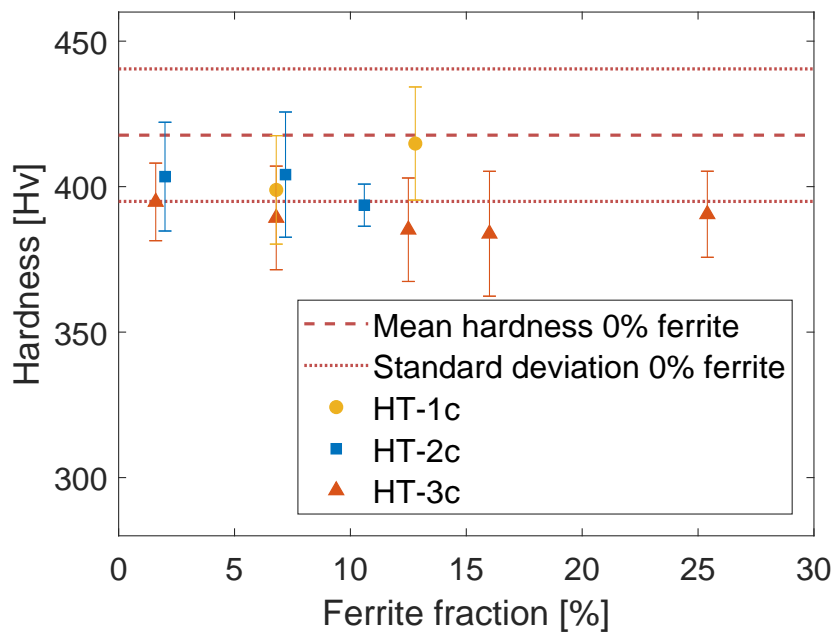


Figure 4.19: Hardness results of heat treatments HT-1c (circles), HT-2c (squares) and HT-3c (triangles). Error bars depict the standard deviation of the 16 measurements per sample. For the 0% ferrite case 32 measurements were used as data of 2 samples from HT-2c and HT-3c, respectively, was combined.

4.4 Micro-hardness

In order to study the effect of prior ferrite on the mechanical properties of bainite, Vickers micro-hardness tests were performed as described in Section 3.7. The results of these tests are shown in Figure 4.19. In this figure, the 0% ferrite case consists of 16 measurements from HT-2c and 16 measurements from HT-3c. These measurements are bundled, as they were all performed in the absence of ferrite. PAGES, if influencing bainite packet size, could also influence hardness. However, this effect can be considered as insignificant [8], especially when differences in PAGES are small (same order of magnitude). All samples that contained a certain fraction of ferrite were subjected to 16 measurements per sample.

It can be seen from Figure 4.19 that the highest hardness is achieved in the samples that do not contain any prior ferrite (red dotted lines). As the ductile ferrite phase is absent and high fractions of bainite and martensite (which are hard phases) are present, it is not surprising that these samples display the highest hardness values. The intercritically annealed samples show hardness values that are slightly lower than the fully austenitised samples, which is explained by the presence of ferrite.

In the range of ferrite fractions that were studied, the ferrite fraction does not seem to have a major influence on the hardness. However, this is thought to be an artifact of the micro-hardness

measuring technique. Indentations are made very locally and the effect of the more ductile ferrite grains may therefore have escaped the measurements, despite the effort to mitigate this effect by measuring 16 points per sample. The inhomogeneous distribution of ferrite grains (banding) may also have had an influence on this, as ferrite grains were often localised in a banded structure. In theory, an increase of ferrite fraction would result in an increase in ductility of the sample. This is one of the main reasons behind the success of dual-phase steels, where the ductility of the steel can be altered by altering the amount of ferrite in the dual-phase microstructure [86]. It is therefore highly recommended that hardness tests in multiphase structures, like the samples in this study, are carried out on a macro scale. In this study samples were small and macro-hardness tests were therefore not a viable option.

The impact of small ferrite fractions on the overall hardness of the material will be small when compared to larger ferrite fractions. As was discussed in Section 4.3.2, in heat treatment HT-3c the smallest ferrite fraction of 2% resulted in the highest acceleration of bainite formation. It is expected that the acceleration of bainite formation by forming/retaining a small fraction of ferrite will not significantly influence the hardness of the final microstructure, and would therefore be advantageous to the heat treatment process. However, more extensive mechanical testing, preferably on the macro scale, is required in order to determine the effects of small ferrite fractions in a bainitic microstructure on the overall mechanical properties of the material.

Chapter 5: Conclusions

In this work the effect of prior ferrite on the bainite transformation kinetics in a Fe-0.2C-3Mn-2Si (wt%) steel was studied. Three different heat treatments were applied. Two comprised an isothermal hold at various temperatures between 835°C and 950°C for 300 seconds, after which slow vacuum cooling with a rate of 2°C/s was used to cool to a bainite formation temperature of 400°C. These two heat treatments differed in heating rate and were heated with 5°C/s and 10°C/s, respectively. The third heat treatment used a heating rate of 1°C/s and lacked the intercritical isothermal hold. Various top temperatures were reached, after which a cooling rate of 30°C/s was used to cool to a bainite formation temperature of 400°C. The heat treatments were conducted in a dilatometer and the resulting microstructure was studied using optical microscopy, scanning electron microscopy and micro-hardness measurements.

During this study several points of interest were found:

- The formation of up to 25% ferrite prior to bainite formation leads to a significant increase in the bainite formation rate. In this way, a reduction in bainite formation time can be achieved.
- For most of the involved heat treatments, smaller prior ferrite fractions (down to 2%) seem to have a higher accelerating effect on the bainite transformation kinetics. However, it was also observed that higher ferrite fractions were needed when a heating rate of 10°C/s was used to achieve a similar effect on bainite formation kinetics as with a heating rate of 5°C/s.
- Due to the formation of prior ferrite, the rather slow start of bainite transformation experienced by fully austenitised samples is accelerated. It is proposed that this can be explained by the increase in preferential nucleation sites for bainite.
- A fast growth of the bainite formation rate to high maxima is observed when prior ferrite is present. It is thought that this can be ascribed to the increased number of bainite sheaves that starts to form simultaneously, increasing the effect of autocatalytic nucleation of new bainite sub-units.
- After reaching a maximum bainite formation rate, the rate decreases again due to carbon enrichment of surrounding austenite and decreasing austenite fraction.

- It is possible to significantly accelerate the formation of bainite by retaining a small fraction of ferrite via an intercritical annealing treatment. Bainite formation times can therefore be shortened without the need for an additional annealing treatment to form ferrite after full austenitisation. This provides the option to save a significant amount of time during the production of steels that contain bainite.
- It was found that a smaller prior austenite grain size is able to accelerate bainite formation.
- It was theorised that to accelerate the formation of bainite, ferrite grains which are evenly dispersed throughout the material and that offer a large interfacial area in comparison to their volume are preferred.
- A change in bainite morphology from degenerated upper bainite to granular bainite was observed when the prior ferrite fraction was increased. This is ascribed to the increase in carbon concentration of austenite with increasing ferrite fractions.
- No significant difference in hardness was observed between the bainitic samples that contained prior ferrite. However, it was theorised that increasing ferrite fractions will lower the hardness of the material. In the absence of prior ferrite slightly harder specimen were produced.

Chapter 6: Recommendations

A few things can be recommended as topics in the event of future research in the field of bainite transformation kinetics. These topics are related to the work in this thesis or are generated by it.

- First of all, it would be interesting to perform a study similar to this one, but with homogenised samples. This will eliminate the effect of banding and may alter the effect that prior ferrite has on the bainite formation kinetics. In this thesis it is already postulated that the accelerating effects will be increased, as prior ferrite grains will be more evenly dispersed (creating a larger ferrite/austenite interfacial area) and manganese and silicon concentrations are more constant throughout the material. Interrupted heat treatments, where bainite formation is only partially allowed, may help to visualise the effect of ferrite/austenite interfacial area.
- A shift in the effect of ferrite fraction on bainite formation kinetics was observed between heat treatments HT-1c and HT-2c, that used heating rates of 5°C/s and 10°C/s, respectively, but were otherwise very similar. As no plausible explanation could be found as part of this work, it is recommended that the effect of heating rate on bainite formation kinetics, in combination with intercritical annealing and ferrite formation during slow cooling, is further studied.
- The effect that prior ferrite, formed after complete austenitisation, has on the bainite transformation kinetics deserves more elaboration. As Ravi et al. [3] already showed, a small amount of ferrite can have an accelerating effect. It would be interesting to see what effect larger prior ferrite fractions have and how the observed accelerating behaviour further develops.
- When the acceleration of the bainite transformation would lead to a significant deterioration of the mechanical properties of the steel, it would be of little use for the industry. It is therefore recommended that the mechanical properties of the ‘accelerated’ bainite are studied in more detail and compared to those of bainite that is formed under conventional conditions (no prior ferrite). This topic was already touched upon in this thesis by performing some micro-hardness tests, but further evaluation of mechanical properties such as tensile strength, macro-hardness and fracture toughness is recommended.

- In this thesis it is suggested that there is a trade-off between accelerating effects and decelerating effects when prior ferrite is formed. Both from a scientific and an industrial point of view it would be attractive to see if an equation could be found that can predict the optimal prior ferrite fraction that would result in the highest acceleration of the bainite transformation. Such an equation could be empirical or scientifically based.
- It is important to note that for this study and the study by Ravi et al. [3] a steel alloy was chosen that did not allow the formation of cementite. As Quidort and Brechet [4] already showed, the formation of cementite can act as an effective carbon sink, which results in a further acceleration of the bainite formation kinetics. The effect of alloying content and its relation to bainite transformation kinetics would thus be a valuable aspect to study.
- Last but not least, for future studies it is recommended that the cause and correction (or prevention) of the measurement error experienced during dilatometry (see Appendix B) is further studied. Depending on the outcome of such a study, this may make future studies more accurate and might result in improved dilatometry hardware or software.

Bibliography

- [1] L. Fielding, “The bainite controversy,” *Materials Science and Technology*, vol. 29, pp. 383–399, 2013.
- [2] C. Garcia-Mateo, F. G. Caballero, and H. K. D. H. Bhadeshia, “Acceleration of low-temperature bainite,” *ISIJ International*, vol. 43, pp. 1821–1825, 2003.
- [3] A. M. Ravi, A. Kumar, M. Herbig, J. Sietsma, and M. J. Santofimia, “Impact of austenite grain boundaries and ferrite nucleation on bainite formation in steels,” *To be published*, vol. -, pp. -, 2019.
- [4] D. Quidort and Y. J. M. Bréchet, “Isothermal growth kinetics of bainite in 0.5% C steels,” *Acta Materialia*, vol. 49, pp. 4161–4170, 2001.
- [5] K. Zhu, H. Chen, J. P. Masse, O. Bouaziz, and G. Gachet, “The effect of prior ferrite formation on bainite and martensite transformation kinetics in advanced high-strength steels,” *Acta Materialia*, vol. 61, pp. 6025–6036, 2013.
- [6] H. Bhadeshia and R. Honeycombe, *Steels: Microstructure and Properties*, ch. 6. Elsevier, 4 ed., 2017. Kidlington, UK.
- [7] H. K. D. H. Bhadeshia, “High performance bainitic steels,” *Materials Science Forum*, vol. 500-501, pp. 63–74, 2005.
- [8] H. K. D. H. Bhadeshia, *Bainite in Steels*. Maney Publishing, 3 ed., 2015. Cambridge, UK.
- [9] W. D. Callister Jr. and D. G. Rethwisch, *Fundamentals of Materials Science and Engineering*. John Wiley & Sons Inc, 2016.
- [10] F. G. Caballero, D. San Martin, C. Capdevila, A. Garcia-Junceda, and C. García de Andrés, *Solid-to-Solid Phase Transformations in Inorganic Materials*, vol. 1, ch. 1: Diffusional Transformations, pp. 707–712. Trans Tech Publications, 2005.
- [11] D. A. Porter, K. E. Easterling, and M. Y. Sherif, *Phase Transformations in Metals and Alloys*. CRC Press, 2009.

- [12] H. Bhadeshia and R. Honeycombe, *Steels: Microstructure and Properties*, ch. 3. Elsevier, 4 ed., 2017. Kidlington, UK.
- [13] G. R. Speich, V. A. Demarest, and R. L. Miller, “Formation of austenite during intercritical annealing of dual-phase steels,” *Metallurgical and Materials Transactions A*, vol. 12, pp. 1419–1428, 1981.
- [14] R. Wei, M. Enomoto, R. Hadian, H. S. Zurob, and G. R. Purdy, “Growth of austenite from as-quenched martensite during intercritical annealing in an Fe-0.1C-3Mn-1.5Si alloy,” *Acta Materialia*, vol. 61, pp. 697–707, 2013.
- [15] F. G. Caballero, C. Capdevila, and C. García de Andrés, “An attempt to establish the variables that most directly influence the austenite formation process in steels,” *ISIJ International*, vol. 43, pp. 726–735, 2003.
- [16] R. R. Mohanty, O. A. Girina, and N. M. Fonstein, “Effect of heating rate on the austenite formation in low-carbon high-strength steels annealed in the intercritical region,” *Metallurgical and Materials Transactions A*, vol. 42A, pp. 3680–3690, 2011.
- [17] T. Nyssönen, P. Peura, and V. T. Kuokkala, “Crystallography, morphology, and martensite transformation of prior austenite in intercritically annealed high-aluminum steel,” *Metallurgical and Materials Transactions A*, vol. 49, p. 6426–6441, 2018.
- [18] A. Navarro-López, J. Sietsma, and M. Santofimia, “Effect of prior athermal martensite on the isothermal transformation kinetics below M_s in a low-C steel,” *Metallurgical Material Transactions A*, vol. 47A, pp. 1028–1039, 2016.
- [19] J. M. Robertson, “The microstructure of rapidly cooled steel,” *Journal of the Iron and Steel Institute*, vol. 119, pp. 391–424, 1929.
- [20] S. J. Matas and R. Hehemann, “The structure of bainite in hypoeutectoid steels,” *TMS-AIME*, vol. 221, pp. 179–185, 1961.
- [21] E. S. Davenport and E. C. Bain, “Transformation of austenite at constant subcritical temperatures,” *Transactions of the American Institute of Mining and Metallurgical Engineers*, vol. 90, pp. 117–154, 1930.
- [22] A. Hultgren, “-,” *Journal of the Iron and Steel Institute*, vol. 114, pp. 421–422, 1926.
- [23] M. Hillert, “Diffusion in growth of bainite,” *Metallurgical Materials Transactions A*, vol. 25, pp. 1957–1966, 1994.

- [24] M. Hillert, L. Hoglund, and J. Agren, "Role of carbon and alloying elements in the formation of bainitic ferrite," *Metallurgical Materials Transactions A*, vol. 35, pp. 3693–3700, 2004.
- [25] D. Quidort and Y. Bréchet, "The role of carbon on the kinetics of bainite transformation in steels," *Scripta Materialia*, vol. 47, pp. 151–156, 2002.
- [26] K. M. Wu, M. Kagayama, and M. Enomoto, "Kinetics of ferrite transformation in an Fe-0.28 mass% C-3 mass% Mo alloy," *Materials Science and Engineering*, vol. A343, pp. 143–150, 2003.
- [27] H. K. D. H. Bhadeshia, "Considerations of solute-drag in relation to transformations in steels," *Journal of Materials Science*, vol. 18, pp. 1473–1481, 1983.
- [28] H. K. D. H. Bhadeshia and D. V. Edmonds, "The mechanism of bainite formation in steels," *Acta Metallurgica*, vol. 28, pp. 1265–1273, 1980.
- [29] F. G. Caballero, C. Garcia-Mateo, M. J. Santofimia, M. M. K., and C. García de Andrés, "New experimental evidence on the incomplete transformation phenomenon in steel," *Acta Materialia*, vol. 57, pp. 8–17, 2009.
- [30] M. Takahashi and H. K. D. H. Bhadeshia, "Model for transition from upper to lower bainite," *Materials Science and Technology*, vol. 6, pp. 592–603, 1990.
- [31] H. K. D. H. Bhadeshia, "A rationalisation of shear transformations in steels," *Acta Metallurgica*, vol. 29, pp. 1117–1130, 1981.
- [32] H. Matsuda and H. K. D. H. Bhadeshia, "Kinetics of the bainite transformation," *Proceedings of the Royal Society A*, vol. 460, pp. 1707–1722, 2004.
- [33] F. G. Caballero and H. K. D. H. Bhadeshia, "Very strong bainite," *Current Opinion in Solid State and Materials Science*, vol. 8, pp. 251–257, 2004.
- [34] H. K. D. H. Bhadeshia, "Nanostructured bainite," *Proceedings of the Royal Society A*, vol. 466, pp. 3–18, 2010.
- [35] C. Garcia-Mateo and F. G. Caballero, "Ultra-high-strength bainitic steels," *ISIJ International*, vol. 45, pp. 1736–1740, 2005.
- [36] J. R. Vilella, "–," *Transactions of AIME*, vol. 140, p. 332, 1940.
- [37] J. Speer, D. K. Matlock, B. C. De Cooman, and J. G. Schroth, "Carbon partitioning into austenite after martensite transformation," *Acta Materialia*, vol. 51, pp. 2611–2622, 2003.

- [38] J. G. Speer, D. V. Edmonds, F. C. Rizzo, and D. K. Matlock, "Partitioning of carbon from supersaturated plates of ferrite, with application to steel processing and fundamentals of the bainite transformation," *Current Opinion in Solid State and Materials Science*, vol. 8, pp. 219–237, 2004.
- [39] B. C. Muddle and J. F. Nie, "Formation of bainite as a diffusional-displacive phase transformation," *Scripta Materialia*, vol. 47, pp. 187–192, 2002.
- [40] A. Saha, G. Ghosh, and G. B. Olson, "An assessment of interfacial dissipation effects at reconstructive ferrite-austenite interfaces," *Acta Materialia*, vol. 53, pp. 141–149, 2005.
- [41] M. Nemoto, *Growth of bainite in an iron-nickel-carbon alloy*, pp. 230–234. Academic Press, 1974. New York, USA.
- [42] R. Le Houillier, G. Begin, and A. Dube, "A study of the peculiarities of austenite during the formation of bainite," *Metallurgical Transactions*, vol. 2, pp. 2645–2653, 1971.
- [43] A. Borgenstam and M. Hillert, *Phase Transformations in Steels*, ch. 13: Kinetics of bainite transformation in steels, pp. 468–501. Woodhead Publishing, 2012.
- [44] W. T. Reynolds, S. K. Liu, F. Z. Li, S. Hartfield, and H. I. Aaronson, "An investigation of the generality of incomplete transformation to bainite in Fe-C-X alloys," *Metallurgical Transactions A*, vol. 21A, pp. 1479–1491, 1990.
- [45] G. R. Purdy and Y. J. M. Brechet, "A solute drag treatment of the effects of alloying elements on the rate of the proeutectoid ferrite transformation in steels," *Acta Metallurgica et Materialia*, vol. 43, pp. 3763–3774, 1995.
- [46] H. J. Lee, G. Spanos, G. J. Shiflet, and H. I. Aaronson, "Mechanisms of the bainite (non-lamellar eutectoid) reaction and a fundamental distinction between the bainite and pearlite (lamellar eutectoid) reactions," *Acta Materialia*, vol. 36, pp. 1129–1140, 1988.
- [47] H. K. D. H. Bhadeshia, "Bainite: Overall transformation kinetics," *Journal de Physique*, vol. 43, pp. 443–448, 1982.
- [48] A. M. Ravi, J. Sietsma, and M. J. Santofimia, "Exploring bainite formation kinetics distinguishing grain-boundary and autocatalytic nucleation in high and low-si steels," *Acta Materialia*, vol. 105, pp. 155–164, 2016.
- [49] M. J. Santofimia, F. G. Caballero, C. Capdevilla, C. Garcia-Mateo, and C. G. García de Andrés, "Evaluation of displacive models for bainite transformation kinetics in steels," *Materials Transactions*, vol. 47, pp. 1492–1500, 2006.

- [50] M. Oka and H. Okamoto, "Variation of transition temperatures from upper to lower bainites in plain carbon steels," *Journal de Physique IV*, vol. C8, pp. 503–508, 1995.
- [51] F. G. Caballero, *Phase Transformations in Steels*, ch. 13: Carbide-free bainite in Steels, pp. 437–467. Woodhead Publishing, 2012.
- [52] H. Föll, *Iron, Steel and Swords*, ch. 9: Science of alloying. University of Kiel. Accessed: 2019-10-14.
- [53] C. Hofer, H. Leitner, F. Winkelhofer, H. Clemend, and S. Primig, "Structural characterization of "carbide-free" bainite in a Fe-0.2C-1.5Si-2.5Mn steel," *Materials Characterization*, vol. 102, pp. 85–91, 2015.
- [54] H. Guo, P. Zhou, A. Zhao, C. Zhi, R. Ding, and J. Wang, "Effects of Mn and Cr contents on microstructures and mechanical properties of low temperature bainitic steel," *Journal of Iron and Steel Research International*, vol. 24, pp. 290–295, 2017.
- [55] Z. Yang, C. Chu, F. Jiang, Y. Qin, X. Long, S. Wang, D. Chen, and F. Zhang, "Accelerating nano-bainite transformation based on a new constructed microstructural predicting model," *Materials Science and Engineering A*, vol. A748, pp. 16–20, 2019.
- [56] Y. Toji, H. Matsuda, and D. Raabe, "Effect of Si on the acceleration of bainite transformation by preexisting martensite," *Acta Materialia*, vol. 116, pp. 250–262, 2016.
- [57] W. Gong, Y. Tomota, S. Harjo, Y. H. Su, and K. Aizawa, "Effect of prior martensite on bainite transformation in nanobainite steel," *Acta Materialia*, vol. 85, pp. 243–249, 2015.
- [58] V. Smanio and T. Sourmail, "Effect of partial martensite transformation on bainite reaction kinetics in different 1% C steels," *Solid State Phenomena*, vol. 172, pp. 821–826, 2011.
- [59] H. Kawata, K. Hayashi, N. Sugiura, N. Yoshinaga, and M. Takahashi, "Effect of martensite in initial structure on bainite transformation," *Materials Science Forum*, vol. 638-642, pp. 3307–3312, 2010.
- [60] S. M. C. van Bohemen, "The nonlinear lattice expansion of iron alloys in the range 100–1600 k," *Scripta Materialia*, vol. 69, pp. 315–318, 2013.
- [61] TA Instruments, "DIL 805 A/D: Quenching and deformation dilatometers." www.tainstruments.com/dil-805ad/, 2019. Accessed: 2019-06-25.
- [62] F. L. G. Oliveira, M. S. Andrade, and A. B. Cota, "Kinetics of austenite formation during continuous heating in a low carbon steel," *Materials Characterization*, vol. 58, pp. 256–261, 2007.

- [63] ASTM International, “E 562: Standard test method for determining volume fraction by systematic manual point count,” 2001.
- [64] ASTM International, “E 384: Standard test method for microindentation hardness of materials,” 2017.
- [65] T. de Cock, C. Capdevilla, F. G. Caballero, and C. García de Andrés, “Interpretation of a dilatometric anomaly previous to the ferrite-to-austenite transformation in a low carbon steel,” *Scripta Materialia*, vol. 54, pp. 949–954, 2006.
- [66] M. Onink, C. M. Brakman, F. D. Tichelaar, E. J. Mittemeijer, S. van der Zwaag, J. H. Root, and N. B. Konyer, “The lattice-parameters of austenite and ferrite in fe-c alloys as functions of carbon concentration and temperature,” *Scripta Metallurgica et Materialia*, vol. 29, pp. 1011–1016, 1993.
- [67] S. J. Lee, K. D. Clarke, and C. J. Van Tyne, “An on-heating dilation conversional model for austenite formation in hypoeutectoid steels,” *Metallurgical and Materials Transactions A*, vol. 41, pp. 2224–2235, 2010.
- [68] J. Wang, P. van der Wolk, and S. van der Zwaag, “Determination of martensite start temperatures in engineering steels part I. empirical relations describing the effect of steel chemistry,” *Materials Transactions JIM*, vol. 41, no. 7, pp. 761–768, 2000.
- [69] S. Chupatanakul and P. Nash, “Dilatometric measurement of carbon enrichment in austenite during bainite transformation,” *Journal of Materials Science*, vol. 41, p. 4965–4969, 2006.
- [70] J. Wang and S. van der Zwaag, “Stabilization mechanisms of retained austenite in transformation-induced plasticity steel,” *Metallurgical and Materials Transactions A*, vol. 32A, pp. 1527–1539, 2001.
- [71] J. Mahieu, J. Maki, B. C. De Cooman, and S. Claessens, “Phase transformation and mechanical properties of si-free cmnal transformation-induced plasticity–aided steel,” *Metallurgical and Materials Transactions A*, vol. 33A, pp. 2573–2580, 2002.
- [72] W. Zhou, T. Hou, C. Zang, L. Zhong, and K. Wu, “Effect of carbon content in retained austenite on the dynamic tensile behavior of nanostructured bainitic steel,” *Metals*, vol. 8, pp. 907–917, 2018.
- [73] B. Dong, T. Hou, W. Zhou, G. Zhang, and K. Wu, “The role of retained austenite and its carbon concentration on elongation of low temperature bainitic steels at different austenitising temperature,” *Metals*, vol. 8, pp. 931–941, 2018.

- [74] S. J. Lee, J. S. Park, and Y. K. Lee, “Effect of austenite grain size on the transformation kinetics of upper and lower bainite in a low-alloy steel,” *Scripta Materialia*, vol. 59, pp. 87–90, 2008.
- [75] L. Y. Lan, C. L. Qiu, D. W. Zhao, X. H. Gao, and L. X. Du, “Effect of austenite grain size on isothermal bainite transformation in low carbon microalloyed steel,” *Materials Science and Technology*, vol. 27, pp. 1657–1663, 2011.
- [76] G. Xu, F. Liu, L. Wang, and H. Hu, “A new approach to quantitative analysis of bainitic transformation in a superbainite steel,” *Scripta Materialia*, vol. 68, pp. 833–836, 2013.
- [77] F. Hu, P. D. Hodgson, and K. M. Wu, “Acceleration of the super bainite transformation through a coarse austenite grain size,” *Materials Letters*, vol. 122, pp. 240–243, 2014.
- [78] S. Sun and M. Pugh, “Manganese partitioning in dual-phase steel during annealing,” *Materials Science and Engineering*, vol. A276, pp. 167–174, 2000.
- [79] S. J. Lee, S. Lee, and B. C. De Cooman, “Mn partitioning during the intercritical annealing of ultrafine-grained 6% Mn transformation-induced plasticity steel,” *Scripta Materialia*, vol. 64, pp. 649–652, 2011.
- [80] A. Nouri, H. Saghafian, and S. Kheirandish, “Effects of silicon content and intercritical annealing on manganese partitioning in dual phase steels,” *Journal of Iron and Steel Research*, vol. 17, pp. 44–50, 2010.
- [81] Y. Toji, T. Yamashita, K. Nakajima, K. Okuda, H. Matsuda, H. Hasegawa, and K. Seto, “Effect of Mn partitioning during intercritical annealing on following γ to α transformation and resultant mechanical properties of cold-rolled dual phase steels,” *ISIJ International*, vol. 81, pp. 818–825, 2011.
- [82] T. Nakagaito, H. Matsuda, Y. Nagataki, and K. Seto, “Effects of partitioning of manganese and silicon during intercritical annealing on transformation behavior and mechanical properties of low alloyed TRIP-assisted steel sheets,” *ISIJ International*, vol. 57, pp. 380–387, 2017.
- [83] K. Radwanski, “Structural characterization of low-carbon multiphase steels merging advanced research methods with light optical microscopy,” *Archives of Civil and Mechanical Engineering*, vol. 16, pp. 282–293, 2016.
- [84] A. Królicka, K. Radwanski, A. Ambroziak, and A. Zak, “Analysis of grain growth and morphology of bainite in medium-carbon spring steel,” *Materials Science and Engineering: A*, vol. 768, p. to be published, 2019.

- [85] G. Spanos, H. S. Fang, D. S. Sarma, and H. I. Aaronson, “Influence of carbon concentration and reaction temperature upon bainite morphology in Fe-C-2 pct Mn alloys,” *Metallurgical Transactions A*, vol. 21, p. 1391–1411, 1990.
- [86] N. Fonstein, *Automotive steels*, ch. 7: Dual-phase steels, pp. 167–216. ArcelorMittal Global R&D, 2017.
- [87] J. Koning, *Samples GEL870 0017*. DEMO TU Delft, 2019. Delft, Netherlands.

Appendix A: Sample Cutting

The following technical drawings were made by Jeroen Konings from DEMO TU Delft [87] and show the sample dimensions, slab dimensions and the manner in which the samples were extracted from the slab.

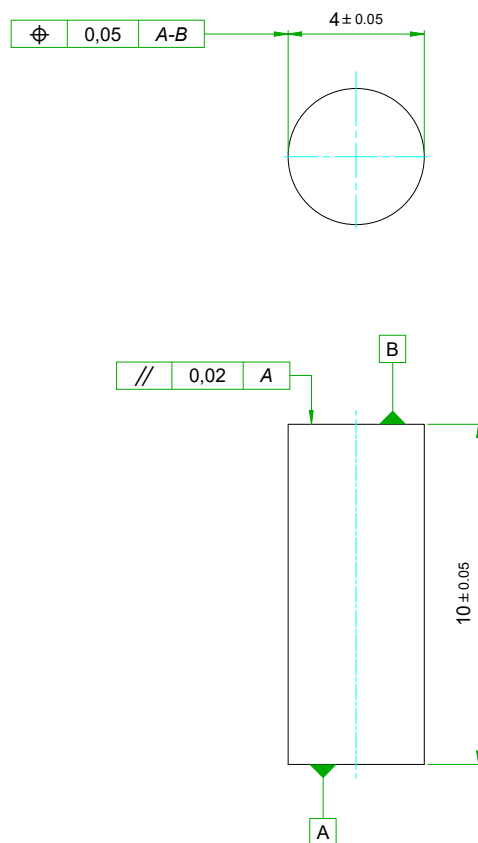
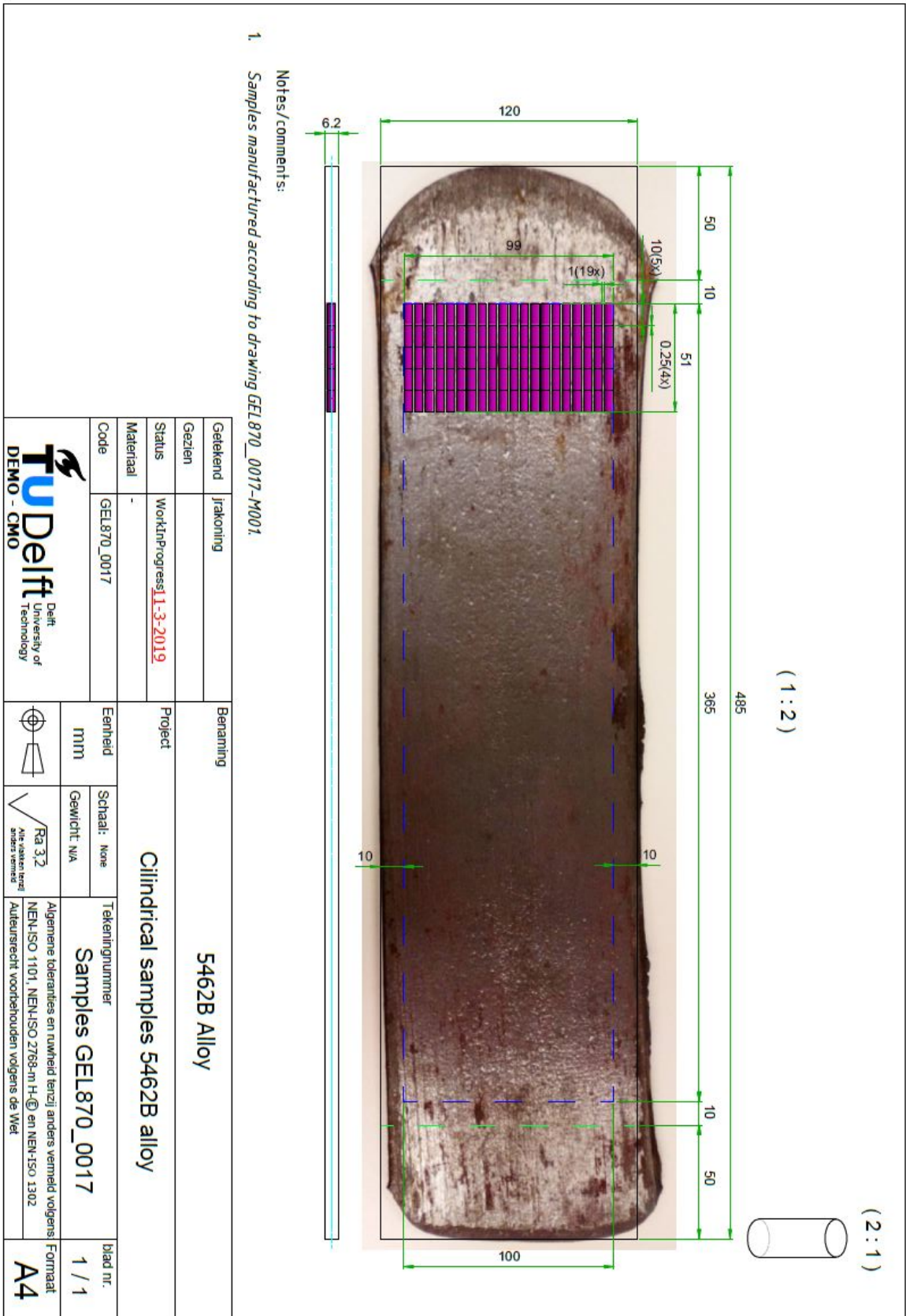


Figure A.1: Drawing GEL870_0017-M001 indicating the dimensions for the dilatometry samples.



Appendix B: Error in Dilatometry Data

In Section 3.3 it was discussed that heat treatments HT-1 and HT-2 used cooling under vacuum conditions. This resulted in a smooth expansion curve during bainite formation, as can be seen from the example in (c) of Figure B.1. However, HT-3 used a higher cooling rate for which He gas was used as coolant. The change of atmosphere introduced an error in the expansion curve during bainite formation, as was briefly discussed in Section 4.3 and is shown in Figure 4.16 and as (a) in Figure B.1.

To understand the cause and extend of the error, additional dilatometry experiments were carried out. One of these experiments consisted of applying heat treatment HT-3c (with 865°C as top temperature) to a sample made from an invar alloy (iron alloy with a high nickel content). This alloy does not transform at 400°C and any expansion/contraction observed at the 400°C isothermal hold would therefore be caused by the measurement error. The result of this experiment is shown as (b) in Figure B.1. As can be seen in the figure, there is indeed some change in expansion, but overall the error is little larger than 1 μm . In addition, it does not show the characteristic ‘jump’ in data at 9 to 10 seconds shown in Figure 4.16, but instead shows a minor peak.

A second dilatometry experiment was carried out with a sample from the same alloy used in this study. Again heat treatment HT-3c with 865°C as top temperature was applied. However, this time the vacuum was not applied after (gas) cooling to 400°C, as it was believed that the activation of the vacuum pump might cause the jump in data. Here it has to be mentioned that the original cooling gas scheme used in heat treatment HT-3 consisted of maximum cooling (thus maximum gas output) until 400°C was reached, after which a small amount of gas was still flowing for 10 more seconds to ensure the temperature remained constant. After these 10 seconds the vacuum pump was turned on, a moment which approximately coincides with the jump in data. It was therefore believed that the activation of the vacuum pump slightly rocks the dilatometer and causes an error in the data. The results of this experiment are shown as (d) in Figure B.1, which shows that the jump in data is still present, although less abrupt. The activation of the vacuum pump itself can therefore be ruled out (although it might cause a small peak, as shown in (d) in Figure B.1 for the invar alloy).

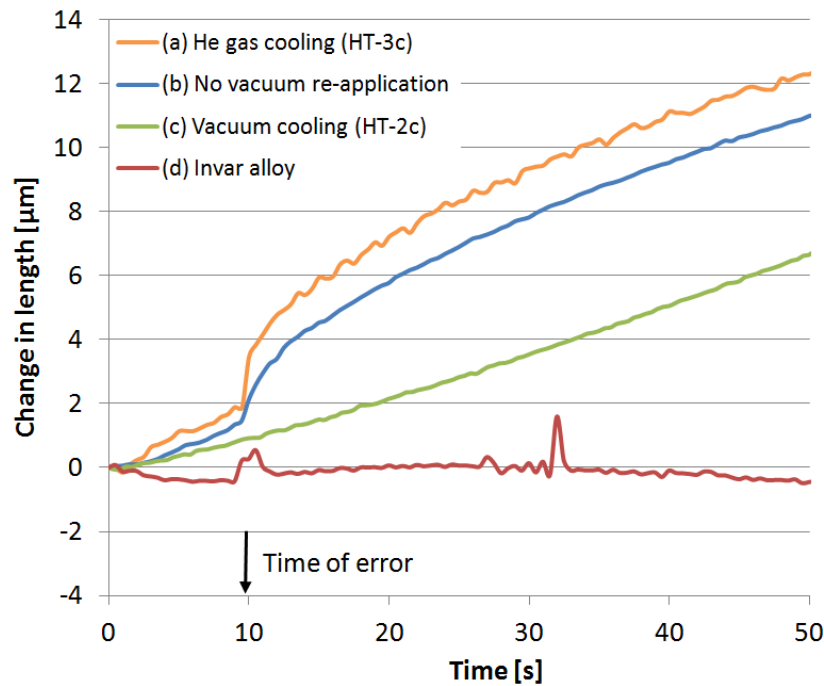


Figure B.1: Comparison of errors in different heat treatments and/or alloys. All heat treatments used a top temperature of 865°C.

Things summarised, the error is not present when vacuum cooling is applied, is present when gas cooling is applied (regardless if the vacuum pump is turned on afterwards) and shows different behaviour when an alloy with no phase transformation at 400°C is used. This leaves only a few options open. It may be that the flow of gas somehow affects the expansion measurements. Instead of just a jump in data it might also be that during the first 10 seconds there is actual expansion present, but that it is only recorded accurately after 10 seconds (which then causes the jump to the right values). The flow of gas may also affect the phase transformation in a way, although this option is less likely as the temperature itself remains constant. The precise cause of the error remains to be determined, something that would be of value for future research.